Reactivity accidents in the GUINEVERE experiment

A. Lafuente,[1] **A. Abanades,**[1] **F. Sordo,**[1] **J.M. Martinez-Val,**[1]
M. Piera,[2] **P. Teles,**[3] **P. Vaz,**[3] **P. Baeten,**[4] **B. Arien**[4]
[1]Universidad Politécnica de Madrid, 28006 Madrid, Spain
[2]Universidad Nacional de Educación a Distancia, 28040 Madrid, Spain
[3]Instituto Tecnologico e Nuclear, EN 10, 2686-953 Sacavem, Portugal
[4]SCK•CEN, Boeretang 200, Mol B-2400, Belgium

Abstract

The GUINEVERE [1] project is a European project in the framework of the FP6 "IP-EUROTRANS" [2]. The IP-EUROTRANS project aims at addressing the main issues for ADS development in the framework of partitioning and transmutation for nuclear waste volume and radio toxicity reduction. The GUINEVERE project is carried out in the context of Domain 2 of IP-EUROTRANS, ECATS, devoted to specific experiments for the coupling of an accelerator, a target and a subcritical core. These experiments should provide an answer to the questions of on-line reactivity monitoring, subcriticality determination and operational procedures (loading, start-up, shutdown, etc.) in an ADS by 2009-2010.

The present study aims at analysing the behaviour of the GUINEVERE experiment in case of accidental reactivity insertion. In particular it investigates, for licensing purposes, the maximum reactivity that can be inserted in the reactor without causing any damage to the core assemblies. This is a complex problem embodying several fundamental mechanisms with different time constants (and therefore, different reaction speeds). First of all, it is worth remembering that neutron flux and thermal power will evolve very fast in a reactivity trip, particularly if the prompt-criticality state is trespassed. This state is defined as the reactor condition in which the prompt-neutron generation rate equals the destruction rate. If this state is reached, delayed neutrons are no longer needed to keep the neutron reaction chain, and the neutron flux evolution becomes extremely fast, and so does the reactor power (even if it at very low levels before the trip).

This paper provides a deeper insight in the two main mechanisms of this physical evolution: the kinetics of the neutron-chain reaction, which becomes divergent and the thermal-mechanical response.

Introduction

Reactivity monitoring and control is a key safety action in nuclear reactors, including subcritical ADS (accelerator driven systems). Experimental and calibration techniques must be adapted to the specific needs of a given reactor family. Although the physics of the problem is the same in all systems, time constants and nuclear and thermal-mechanical data change from one situation to another. Moreover, some reactivity variations can be negative, as some of the used in ADS to keep the subcritical regime [3]. In this case, the proposed method to monitor reactivity with absolute measurements is based on ultra-short interruptions of the accelerator beam. The subsequent neutron flux decay is unambiguously related to the absolute level of subcriticality. Those interruptions also convey a decay in thermal power in the subcritical reactor. The dynamic response associated to those transients has been analysed in other studies [4].

The purpose of this new task is different, because it addresses the onset of positive reactivity variations (reactivity trips) in a very small power critical reactor before the trip (zero-power reactor, not accounting for active cooling). Specifically, the present study aims at analysing the behaviour of the GUINEVERE facility in case of an accidental reactivity insertion. This approach opens the possibility of setting up a new framework within which it will be possible to compare and benchmark results, guaranteeing the reliability of the licensing process.

In particular, we intend to investigate the maximum reactivity insertion rate that can be applied without causing any damage to the core assemblies. This is a complex problem embodying several fundamental mechanisms with different time constants (and therefore, different reaction speeds). First of all, it is worth remembering that neutron flux and thermal power evolve very fast in a reactivity trip, particularly if the prompt-criticality state is trespassed. This state is defined as the reactor condition in which the prompt-neutron generation rate is equal to the destruction rate. If this state is reached, delayed neutrons are no longer needed to keep the neutron reaction chain, and the neutron flux evolution becomes extremely fast, and so does the reactor power (even if it is at very low levels before the trip) with a resulting thermo-mechanical response.

In the following section a deeper insight on the physical phenomenon involved in reactivity perturbations will be given attending both the neutron kinetics and the thermo-mechanical response. In a subsequent section the whole problem is characterised, including the consideration of different approaches, the safety criteria considered and the evaluation of feedback effects. The data and parameters used in the calculations will then be presented. The main results will be compiled and a sensitivity analysis will be performed in order to determine the envelope to be used for the core certificate procedure. Finally, some conclusions will be presented including some guidance for establishing the most restrictive safety criteria.

Physical phenomena in reactivity trips

There are two main mechanisms in this physical evolution:

- the kinetics of the neutron-chain reaction, which becomes divergent;
- the thermal-mechanical response.

This study can entail great difficulties due to the high non-linear nature of the problem and finding ways of simplifying it arises as a matter of importance. A description of the approach followed can be found in the next lines.

Nuclear reactions (mainly fission) will produce a heat source (mainly in the fuel) and a thermal transient will begin as the power evolution starts. For the sake of easiness we will assume this power evolution governed by a point-kinetic model without shape function recalculation [5].

The thermal transient is characterised by the Fournier dimensionless number [6], F_o, defined as:

$$F_o = \frac{\alpha t}{L^2} \tag{1}$$

where α stands for the thermal diffusivity (m^2/s), t is time and L is the characteristic length of the problem (radius R, in a fuel rod). For a cylinder without an active cooling in its surface (Biot numbers,

Bi << 1) the Fourier number for the duration of a transient is about 10. This means that for times shorter than:

$$t_t = \frac{10\,R^2}{\alpha} \tag{2}$$

most of the thermal energy remains inside the fuel rod. For the GUINEVERE case, with $\alpha = 0.1125$ cm²/s and $R = 0.628$ cm, the transient time t_t is around 35 s. If the neutron flux evolution is much faster than the speed of the thermal transient, as in our case, the increase in the fuel temperature (that will fulfil a flat distribution) will be given by:

$$\Delta T_f = \frac{E}{V\,\rho\,C_f} \tag{3}$$

where E is the total thermal energy released along the transient, V is the fuel rod volume, ρ is the density and C_f the fuel specific heat. In turn:

$$E = \int_0^t c\,\Sigma_f\,\phi(t)dt \tag{4}$$

where c is the conversion factor between the fission rate and thermal power (3.1×10^{-11} J/fission).

Now, if the perturbations are shorter than the characteristic transient time (in our case ~35 s), the temperature variations will be very localised. As most of the energy is released inside the fuel, very large temperature variations can take place in its inner part without the outer part even noticing the change. In other words, a fuel rod can be considered adiabatic, and 100% of the prompt fission energy is deposited inside of it. This is, at least conceptually, a simplified approach that reduces the analysis to the resolution of one single Eq. (3).

Besides this power evolution two other effects will also follow: mechanical expansion and Doppler broadening. Its analysis falls outside the scope of this survey and only a few words will be said in this sense. The thermal expansion of the fuel will be assumed to follow the law:

$$R(t) = R_0(1 + \beta\,\Delta T_f) \tag{5}$$

β being the linear expansion coefficient. This is a very important effect, for two reasons at least. First, the expansion of the fuel can lead it to crash against the cladding and can break it, but is not a matter of concern for GUINEVRE since the fuel rods will not be cased. Besides, the fuel itself can suffer from breaches, and the air gap closure could modify the heat transfer mechanism.

But the thermal expansion also conveys a feedback effect into the reactivity. Take into account that macroscopic cross-sections of neutron reactions depend on density, as:

$$\sum_{ix} f_i\,\rho\,\sigma_x \tag{6}$$

σ_x being a type of microscopic cross-section (fission, capture, scattering) and I the isotope; f_i is the isotope abundance in the fuel, and ρ is its density. The latter is not constant. It changes along a thermal expansion as:

$$\rho(t) = \rho_0(1 + \beta\,\Delta T_f)^{-3} \tag{7}$$

which in general conveys a decrease in reactivity and a small increase in neutron leakage.

Another very important feedback effect in the kinetic evolution is the Doppler broadening, which corresponds to an increase in the neutron captures in ^{238}U, as temperature increases. A lot of literature has been written about it [7] and is well known how the effect decreases as fuel temperature increases. For our study we will merely show the assumed law followed by the combined effect of mechanical expansion and Doppler broadening calculated by means of MCNPX [8]:

$$\frac{\partial}{\partial T} K_{eff}(T_f) = -\frac{0.02617}{T^{3/2}} - 5 \cdot 10^{-7} \tag{8}$$

Characterisation of the problem

The point-kinetics equations involve the determination of the total reactivity $\Delta\rho$ of the core. This reactivity is the sum of two contributions: the inserted reactivity $\Delta\rho_I$ and the feedback reactivity $\Delta\rho_F$, which comes from the Doppler and the density effects on the fuel, as will be explained in the next section. For the inserted reactivity $\Delta\rho_I$ in transient conditions, we consider two phases:

- Reactivity insertion consecutive to an accidental control rod withdrawal. This reactivity insertion is represented by means of a reactivity ramp.
- Reactor scram: the power excursion resulting from the reactivity insertion is detected when the reactor power reaches a threshold value (500 W). A signal is then sent to the scram system to shut down the reactor and the effective safety rod insertion occurs with a delay of 0.3 seconds. During this delay the reactivity ramp is going on. The safety rods fall down by gravity and the inserted anti-reactivity evolves according to a law involving the safety rod position.

This model determines the core power variation during the reactivity insertion transient, assuming that the shape of the total neutron flux distribution in the core, and therefore the shape of the power density distribution are preserved throughout the whole transient. To know the response of the hottest fuel assembly in its midplane and address the safety study, we should just multiply the flux amplitude, obtained from point kinetics, by the peak factor, calculated for the initial condition by means of MCNPX (since the shape will remain constant).

Attending to the description of the accidents, the problem could be studied in the following way: The possible (reactivity insertion rate, initial power) pairs should be those in which the maximum allowable temperature for the fuel should never be reached. In the first instance, one could impose the safety criterion over the fuel melting point, but if we consider that materials will suffer thermal expansion, and that the gap that separates the fuel from the lead could disappear, a more conservative safety criterion could be reformulated impeding the temperature of the outer surface of the fuel element go above the lead melting point. As a consequence, this thermal constraint should be complemented by at least one more; the integrity of the air gap against materials expansion to avoid hot spots and local melting in the lead block. The question is then how to fix the allowable (velocity, initial power) pairs to fulfil the safety criteria during the accidents.

The temperature driven safety criterion can be addressed with the adiabatic fuel rod model explained before. Nevertheless, the integrity of the air gap will need a more complex model since, due to the introduced simplifications in the former approach, all the elements except the fuel have been removed from the calculation. For this reason we will perform this study by means of the ANSYS [9] commercial code with the added value of being able to validate the models used up to this moment.

Data

For this study, only one core configuration has been studied and the geometric data has been taken from [10]. It is the core configuration without a central hole, with 88 standard fuel assemblies and reflector.

All the neutron point kinetics parameters have been re-evaluated for this study using MCNPX and based on the ENDFB-VII [11] neutron data libraries previously compiled with NJOY 99.259 [12]. These values can be grouped into four categories:

- Point kinetics parameters such as delayed neutron fraction, decay constants, mean generation time and k_{eff} (respectively 700.11 pcm, 0.45 s^{-1}, 0.458 μs and 1.01698).
- Anti-reactivity of the control rods as a function of the rod position although this correlation will have a negligible contribution, since our results depend mainly on the reactivity ramp regime. For the calculations the value provided by SCK was used.
- The feedback reactivity caused both by Doppler and fuel expansion already addressed (with a value for C_d = 0.02617).
- Peak factor for the hottest fuel assembly which gives a $\rho^{max}_{power}/P_{total}$ ratio equal to 29.81 m^{-3}.

The thermo-physical properties of the different materials (uranium, lead, nickel, stainless steel, air) were obtained from [13]. It is worth remarking that when using the simplifications proposed in this document only the properties of uranium will be useful. This hypothesis, as we already described, made the problem easier, but also simplified the problem in such a way that the mechanical part could not be addressed. Since we are also interested in the thermo-mechanical response of the system, all the properties of the materials related with this thermo-mechanical response where used.

Table 1: Mechanical properties of different materials

	Young's Modulus	Poisson's Ratio
UO_2	210.2 GPa	0.28
Ni	170 GPa	0.312
Lead	16.1 GPa	0.44
SS AISI 304L	200 GPa	0.29

Operational data such as room temperature, initial temperature in the core, etc. can be found in Ref. [13].

Results and discussion

Results were calculated for the configuration described, although the major differences between this geometry and others will be in the neutron point kinetics parameters.

As a first step, a parametric study was performed, in order to constrain the values that our initial power and the reactivity extraction velocity can take. To do so, we will begin comparing our results, calculated following the described simplified methodology, but using some point kinetic parameters calculated by SCK•CEN in previous studies. This will give us an idea about the degree of convergence of both methodologies.

Once we have analysed the validity of this method, we can undertake a more sensitive analysis to assess the influence of the different parameters, like for instance the ones we calculated, on the results. Finally, we can address the gap closure issue by means of a commercial code called ANSYS at the same time we compare results with the rest of the methodologies.

Method comparison

It is worth remembering that when we begin to insert reactivity in the system the power will rise following, in a first approach, a point kinetic response. The faster the reactivity is inserted, the sooner we reach the power threshold where the scram signal is ordered. Because the GUINEVERE experiment facility will be cooled by means of the natural convection of air, this value was imposed at 500 W. Although the safety control rod insertion will be ordered in that moment, it will not be effective before a time span of 0.3 seconds, and it is because of this delay that the system will suffer a rampant increase of power and, thus, energy, that could lead to temperatures above the melting point. Moreover, when the anti-reactivity of the control rods is introduced, and power suddenly drops, temperatures will still rise until all the accumulated energy begins to be released (which will happen around the characteristic thermal time). So, understanding why reactivity insertion velocity has a main influence in this accidental situation is straightforward. The slope of the power time derivative will be higher if velocities increase. Another free parameter is the initial value of the core power P_0, which heavily influences the results as it will be seen further down. Finally, in all these analyses, the reactivity feedbacks play an important role since, without considering them, the system would be out of control once prompt-criticality was reached.

Figure 1 shows the results. The idea is to analyse the convergence of both approaches. What we see in this figure is a contour plot where the iso-curves of fuel temperature (plotted in black solid line) are shown as a function of the initial power and the reactivity insertion velocity. The red solid line is the temperature limit iso-curve, which corresponds to a value of 325°C, and separates two regions. Above, we have all the possible configuration states, defined by their initial power and reactivity insertion velocity that fulfil, during all the accidental situations, the melting point safety conditions.

Figure 1: General results for different initial powers and velocities

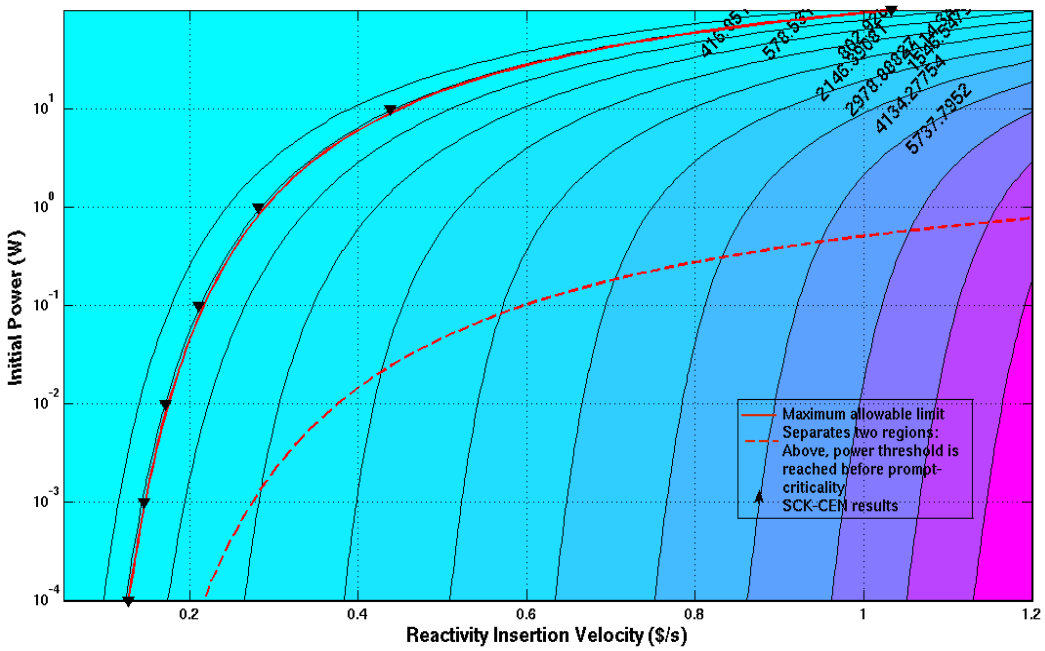

Another interesting information, that should be taken into account, is depicted in the plot with slashed lines that separate the two domains. Once more, above, we have all the phase configurations in which prompt-criticality is reached after the 500 W threshold. This has a considerable importance, since after that point, even when the increase is muffled by feedback effects, power will increase very fast. The later we reach that point, the better, in order to avoid dangerous situations. Nevertheless, this criterion is, as we can appreciate, less restrictive than the first one and will not impose additional constraints. Finally the black triangles show results obtained by SCK•CEN research group using a different methodology and is obvious the high degree of convergence.

Sensitivity analysis

To determine the envelope to be used for the core certificate procedure, a sensitivity analysis has been performed where the effect of the variation of the main kinetic parameters, such as the mean generation time, the delayed neutron fraction or Doppler coefficient has been considered. This will be defined by taking the most conservative values for the various parameters involved in the model.

Results showed that kinetic parameters can be grouped in two categories, depending on whether they have or not any influence in the performed parametric study to calculate the reactivity insertion velocity limits. From the whole, two of them – the mean generation neutron time and the delayed neutron fraction – have a negligible impact. As analysed, both force the reactivity insertion velocity rate limit to have a minimum whatever the value they take. In other words the higher the delayed fraction is, or the lower the mean generation is, the system will never go beyond a minimum which will become the most unfavourable situation threshold.

On the other hand, the Doppler feedback coefficient and the mean decay constant should be considered more seriously. The former will not find any convergence asymptote and the lower the coefficient is the lower the reactivity insertion velocity should be. The latter, after analysing the results, should specifically be considered when having low initial powers, since its effect is only noticeable in that case. Nevertheless, from all the kinetic parameters, this one can be determined with a better accuracy than the others and should never have those degrees of uncertainty. Anyway, we hereby conclude that the stress should be put in the determination of these two values for a correct characterisation of the problem, with a special effort in the determination of the Doppler coefficient.

Thermo-mechanical response

As we have explained in previous sections, the new methodology, proposed by our group, even when it has been demonstrated to be as accurate and conservative as the other, has some drawbacks. To understand this, just remember that in our approach, after proving that the fuel rod could be considered adiabatic (because of its high characteristic transient time), the rest of the geometry could be neglected. This assumption simplified the problem a lot. So much, that the closure of the gap issue could not be addressed because the geometry beyond the fuel rod had been removed.

To overcome this problem the full geometry had to be considered and the lack of validity of the first proposal led to the use of a different code called ANSYS. With it, we would not only be able to perform these calculations with the correspondent added value but also to cross-check once more the previous results concerning the melting point safety criteria obtained by other methodologies.

Assuring the integrity of the gap will be necessary since, if the Ni cladding clashes with the stainless steel lead envelope, it could appear local melting because of the hot spot. From Figure 2 it can be seen that the risk of having the closure of the gap is very low and does not add real problems. The red line and black stars correspond to the melting point safety limits as explained before. The blue line shows the different (power, velocity) pairs for which the gap width was reduced from 0.2 mm to 0.14 mm. This is just a reference value to prove that the other safety criteria are more restrictive than that one that, besides, pulls in a different direction.

Figure 2: Iso-curves for different reactivity insertion velocity limits

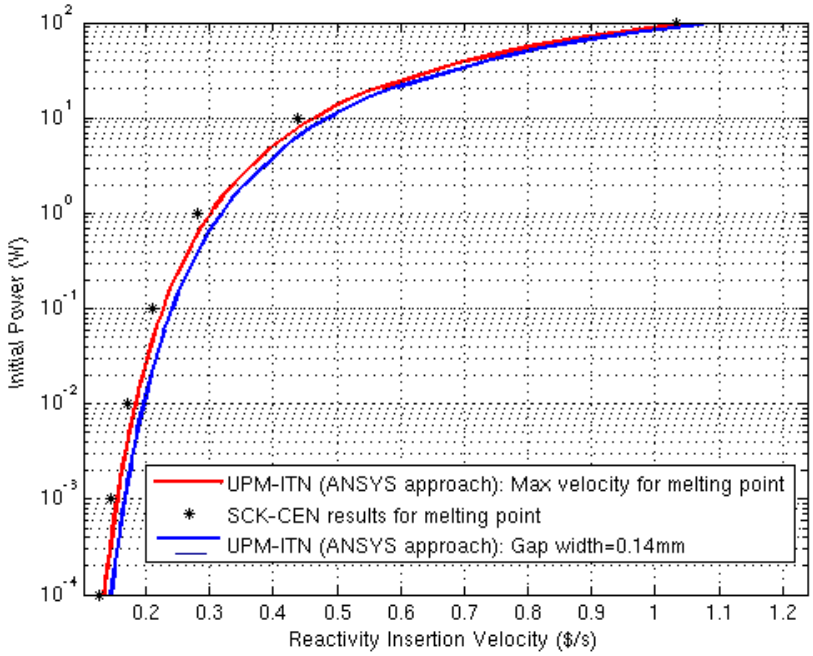

Conclusions

A physical model including thermal treatment and neutron point-kinetics calculations was developed to evaluate the maximum rate of reactivity insertion that can be accepted in GUINEVERE. This was performed using a new conceptual approach, different from those considered in previous works, with the advantage of leading to an easier understanding of the problem. Boundary conditions were imposed on a different basis, attending to physical criteria, in contrast to the former geometrically-based formulation, and its validity has been proven with the GUINEVERE core configuration number 1. Due to the limitations of this first methodology to address the thermo-mechanical part of the study, a second analysis was performed by means of a commercial code that, aside from giving information about the gap closure, was useful to validate the previous models.

Apart from introducing this new methodology, the purpose of this research was to identify, from the safety point of view, the maximum reactivity insertion rate as a function of the initial core power. Two safety criteria where considered. The first one was, regardless of its high degree of conservatism, that the temperature at the surface of the fuel rod may not exceed the lead melting point. The second was the diameter of the fuel rod should never be larger than the distance between two lead blocks.

For this purpose, all the neutron point kinetics parameters have been re-evaluated using MCNPX, and were based on ENDFB-VII neutron data libraries previously compiled with NJOY.

Regarding the validation of the method, the study shows a great degree of convergence with the SCK results and, moreover, with those obtained by means of a commercial code. The higher difference between our approach and the one undertaken in the former study was around a 5% (when using ANSYS with our calculated parameters)

A sensitivity analysis was performed in order to determine the envelope to be used for the core certificate procedure although the conservatism of our hypothesis is by itself a guarantee of reliability. The analysis was mainly focused on the point-kinetics model. It revealed that, except for the Doppler coefficient and the mean decay constant, the impact of these parameters has no influence in the parametric study we performed in order to calculate the reactivity insertion velocity limits.

Finally, we demonstrated that the most conservative criterion comes from the fuel temperature melting point.

Acknowledgements

The authors appreciate the efforts of all the scientists and institutions involved in EUROTRANS, as well as the financial support of the European Commission FP6 IP-EUROTRANS/ECATS project. We also thank CesViMa (Spain) for the access to the Magerit IBM-BladeServer supercomputer. Fruitful discussions and knowledge transfer with M. Yaksh are gratefully acknowledged.

References

[1] Aït Abderrahim, H., *et al.*, "The GUINEVERE-project at the VENUS Facility", *Proceedings of Utilisation and Reliability of High Power Proton Accelerators*, Mol, Belgium, 6-9 May 2007.

[2] Van Goethem, G., *et al.*, "Euratom Innovation in Nuclear Fission: Community Research in Reactor Systems And Fuel Cycles", *Nuclear Engineering and Design,* Vol. 237, Issues 12-13, also in *18th International Conference on Structural Mechanics in Nuclear Engineering*, July 2007, pp. 1486-1502.

[3] Perez, R.B., R.S. Boot, "Excitation of Neutron Waves by Modulated and Pulsed Sources", *Proceedings of the Symposium on Pulsed Neutron Research*, Karlsruhe, 10-14 May 1965, Vol. II, IAEA, Vienna, pp. 701-728 (1965).

[4] Lafuente, A., *et al.*, "Dynamic Response of an Accelerator-driven System to Accelerator Beam Interruptions for Criticality", *Nuclear Instrum. & Meth.* A, Vol. 591, Issue 2, 21 June 2008, pp. 327-337.

[5] Henry, A.F., *Nuclear-reactor Analysis*, MIT Press Cambridge, MA (1975).

[6] Chapman, A.J., *Heat Transfer*, Collier-Mcmillan, N.Y. (1984).

[7] Bell, G., S. Glasstone (Eds.), *Nuclear Reactor Theory* (1970).

[8] Pelowitz, D.B. (Ed.), *MCNPX Users Manual (2.5.0)*, Los Alamos National Laboratory, April 2005.

[9] ANSYS, *1999 ANSYS Elements Reference, ANSYS Release 5.6*, ANSYS Inc. (1999).

[10] Aoust, Th., *GUINEVERE: études de sûreté, modélisation neutronique*, report SCK•CEN-ThA/tha-3910.B045003 – 516/07-19, 6 December 2007.

[11] Chadwick, M.B., P. Oblozinsky, M. Herman, *et al.*, "ENDF/B-VII.0: Next Generation Evaluated Nuclear Data Library for Nuclear Science and Technology", *Nuclear Data Sheets*, Vol. 107, pp. 2931-3060 (2006).

[12] MacFarlane, R.E., D.W. Muir, *The NJOY Nuclear Data Processing System Version 91*, LA-12740-M, Los Alamos National Laboratory (1994).

[13] Arien, B., P. Baeten, *Envelope Determination for Core Certificate Procedure: Analysis of Linear Reactivity Insertion Excursion in the GUINEVERE Experiment*, internal report.

An analytical solution for a simple time dependent neutron transport problem: Shutdown of the external source

B. Merk
Institut of Safety Research
Forschungszentrum Dresden
Rossendorf, Germany

Abstract

An analytical approximation solution for the shutdown of an external source in a homogeneous subcritical reactor problem is developed. The problem is described through an approximation of the Boltzmann transport equation, the Telegrapher's or time dependent P_1 equation. The analytical approximation solution to the problem is expressed in terms of a Green's function expansion. The differences between the solution for the Telegrapher's equation and the diffusion equation without separation of space and time are discussed.

Introduction

The space-time behaviour of the neutron flux in an accelerator-driven system (ADS) is matter of different actual and planned experiments (MUSE [1,2], Yalina [3], SAD [4], Guinevere [5]). The analysis of these experiments is based on the standard methods [2,3] known for experiments in critical reactors. These standard methods are based on the point kinetics equations [6,7] and therefore related to the diffusion approximation with separation of space and time. Especially in accelerator-driven systems with their strong external neutron source one of the major limitations of the diffusion approximation is violated and separation of space and time is not possible. The idea of handling this problem by solving the time dependent Telegrapher's has already been demonstrated for the switch on of the external source [8,9]. Especially the shutdown of the source in a steady-state operating ADS system is a very important problem. This kind of transient could be used for the determination of criticality or better subcriticality during ADS operation. During normal operation accruing short trips of the accelerator offer this possibility.

Background: Telegrapher's equation vs. diffusion equation

The correct P_1 approximation to the Boltzmann equation is not the first order diffusion equation (1), but the second order equation (2), which is called the "Telegrapher's equation". The general solution of the Telegrapher's equation shows the phenomenon of retardation; that is, the solution has a well defined wave front, in addition to a residual disturbance which persists at all points traversed by the wave front [10]:

$$\frac{1}{\mathrm{v}}\left(1+3D\Sigma_a\right)\frac{\partial\phi}{\partial t}=D\Delta\phi-\Sigma_a\phi+S \tag{1}$$

It is a well known property of the diffusion equation that an instantaneous source immediately produces a disturbance at all points in space; that is, the propagation velocity is infinite [10]:

$$\frac{3D}{\mathrm{v}^2}\frac{\partial^2\phi}{\partial t^2}+\frac{1}{\mathrm{v}}\left(1+3D\Sigma_a\right)\frac{\partial\phi}{\partial t}=D\Delta\phi-\Sigma_a\phi+S \tag{2}$$

These two excerpts taken from Weinberg, Wigner summarise the major difference in the time behaviour between the diffusion equation and the Telegrapher's equation for the use in time dependent reactor physics. This difference does not have anything common with the often mentioned and well known differences in static reactor physics; that is, the slightly incorrect k_{eff} especially for small systems with an important role of neutron losses out of the system.

Diffusion equations which arise in mathematical physics usually are approximations to Boltzmann-type equations in which the mean free path is assumed vanishingly small but in which the diffusion coefficient is finite; in neutron diffusion, on the other hand, the mean free path is usually so large (several centimetres) that the existence of the wave front in the time dependent diffusion equation cannot always be ignored [10].

Especially in cases where measurements of heavy changes in the neutron flux are carried out at very short time scales the influence of the wave front cannot always be ignored. This is typically for experiments in accelerator-driven systems where the strong external neutron source is started or shut down.

Solution with Green's functions

Green's function solutions for the telegrapher's equation are already known from former studies and other scientific areas. Solutions are already published for the Telegrapher's equation for problems of thermal conduction in finite media in combination with ultra-short laser pulses [11,12] and for the case of the start-up of an external neutron source [8,9]. The development is started with the dimensionless version of the Telegrapher's equation:

$$\frac{\partial^2\Phi}{\partial\tau^2}+a\frac{\partial\Phi}{\partial\tau}+b\frac{\partial^2\Phi}{\partial\xi^2}+c\Phi=s \tag{3}$$

with the following abbreviations:

$$a \equiv 1+\frac{\Sigma_a}{\Sigma_{tr}}, \quad b \equiv -\frac{1}{3}, \quad c \equiv \frac{\left(\Sigma_a - \nu\Sigma_f\right)}{\Sigma_{tr}}, \quad s \equiv \frac{S}{\Sigma_{tr}}, \quad \tau \equiv \nu\Sigma_{tr}t, \quad \xi \equiv x\Sigma_{tr}, \quad \Phi \equiv \phi(x,t)-\phi_0, \quad la_n \equiv \frac{n\pi}{R}$$

The solution is gained for the case of a subcritical system with an external source in form of a Heaviside function (see Figure 1 for illustration). The source is shutdown at time point $t = 0$ and has the spatial dimension of $\Delta\xi$. The function:

$$S \equiv -\frac{s}{\Delta\xi} Heaviside(\tau)$$

is used to compensate for the in the steady state solution appearing constant external source:

$$\Phi = \Phi_0 + \frac{s}{Rc} - \frac{1}{2}\frac{se^{\left(-\frac{(a+sq_1)\tau}{2}\right)}(sq_1 - a)}{Rsq_1 c} - \frac{1}{2}\frac{se^{\left(-\frac{(a-sq_1)\tau}{2}\right)}(sq_1 + a)}{Rsq_1 c}$$
$$+ 2s\cos(\lambda_n\xi)\sin(\lambda_n\Delta\xi)\sum_{n=1}^{\infty}\frac{-1+e^{\left(-\frac{a\tau}{2}\right)}\cos\left(\frac{sq_2}{2}\tau\right)+\frac{a}{sq_2}e^{\left(-\frac{a\tau}{2}\right)}\sin\left(\frac{sq_2}{2}\tau\right)}{R\left(b\lambda_n^2 - c\right)\Delta\xi\lambda_n} \qquad \text{in } 0 < \xi < R,\ \tau > 0 \qquad (4)$$

with:

$$sq_1 \equiv \sqrt{a^2 + 4c}$$

$$sq_2 \equiv \sqrt{-a^2 + 4b\lambda_n^2 - 4c}$$

and the steady state neutron flux distribution with operating external neutron source:

$$\Phi_0 \equiv -\frac{s}{Rc} + \sum_{n=1}^{\infty}\frac{2s\cos(\lambda_n\xi)\sin(\lambda_n\Delta\xi)}{R\left(b\lambda_n^2 - c\right)\Delta\xi\lambda_n}$$

The solution for the space-time dependent neutron flux [Eq. (4)] is created out of three different parts: the first part represents the steady-state solution with operating external source, the second part (rest of the first row) represents a global change in the neutron flux, while the third part (starting from the sum sign) represents the space-time dependent change in the neutron flux.

Figure 1: Qualitative sketch of the external source shut down at $t = 0$, spatial dimension of $\Delta\xi$ (front half of a symmetric system)

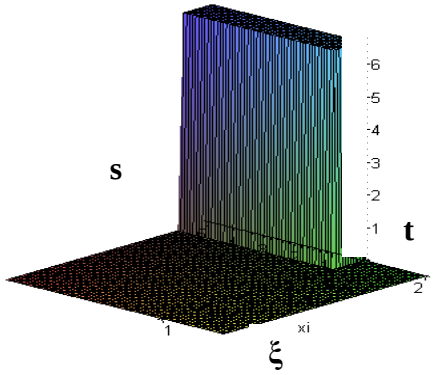

Discussion of results

The evaluation of the results is carried out on the basis of the qualitative results (shown in Figures 2 and 3) for a one-dimensional system with constant neutronic material properties over space and time. Figure 2 shows the transient space-time dependent neutron flux. The transient is started from steady state (on the time axis for $t < 0$) at $t = 0$ by shutting down of the external neutron source like that

presented in Figure 1. The steady-state distribution is given by the final asymptotic distribution reached sufficiently long after the start-up of the external neutron source [8]. The neutron flux especially in the centre of the symmetric system where the influence of the source is strongest decreases rapidly immediately after the shutdown of the external source. The neutron flux change is distributed in a short time period over the entire system. After roughly 0.005 s has the neutron flux died out over the complete system for this case without production of delayed neutrons. Naturally this behaviour is unrealistic because delayed neutrons appear in every today realistic nuclear system. This fraction of delayed neutrons leads to much longer time periods needed for the shutdown of the system.

Figure 3 shows once more the space-time behaviour of the neutron flux but this time normalised with the steady-state neutron flux distribution to highlight the space-time variation especially in the outer area of the system. The plateau in the beginning of the transient demonstrates the time delay occurring in the outer area. The plateau exists longer the bigger the distance to the source in the centre is. This effect can only be observed in a solution of the time dependent transport equation, since exactly this effect would be dropped by solving the diffusion equation due to the infinite propagation velocity of flux change in this approximation. The effect of the finite propagation velocity leading to a real non-separable space-time behaviour can be observed throughout all the time in Figure 3. It leads to a different time evolution of the normalised neutron flux at every point in space.

Figure 2: Qualitative sketch of the one dimensional space-time dependent neutron flux for the first 0.0025 s after shutdown of the external source (at *t* = 0) in a before steady-state operating system (dimensionless co-ordinates and time)

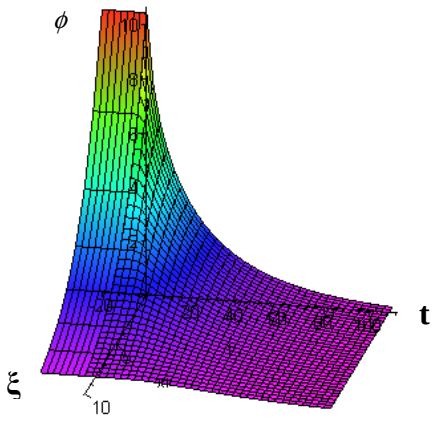

Figure 3: Qualitative sketch of the normalised change of the one-dimensional neutron flux in space and time for the first 0.005 s after shutdown of the external source (at *t* = 0) in a before steady-state operating system (dimensionless co-ordinates and time)

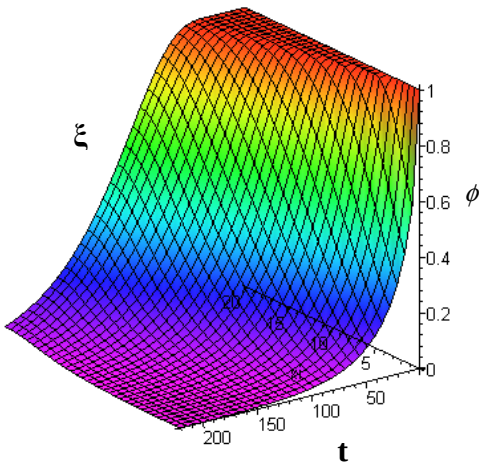

Conclusion

An analytic approximation solution for the Telegrapher's equation in one dimension for a subcritical system with external neutron source, but without delayed neutron production is presented. This solution of the correct P_1 approximation to the time dependent Boltzmann equation shows the phenomenon of retardation – a well-defined wave front and a residual disturbance at all point traversed by the wave front. Therefore this solution offers additional information compared to the well known time dependent diffusion approximation. This information is very valuable in cases where detailed information on the short time behaviour of a system is needed. These kinds of analytical solution can be very helpful especially in experimental set-ups. In kinetic experiments often measurements are performed in the time scale below the delayed neutron production down close to the time scale of prompt neutron production.

With this developed approximation solution a first step performed for an improved method for the analysis of typical ADS experiments on the basis of the transport equation. It is still an approximation for the shutdown of the external neutron source in a system with constant material properties. Nevertheless it is a significant improvement compared to the currently used methods based on point kinetics. Furthermore is this transient foreseen to be used for the standard method for the observation of the subcriticality.

Some further steps are needed for the practical use: consideration of the delayed neutron source by Multiple Scale Expansion [14,15] and maybe a more dimensional solution on the basis of the synthesis method [16].

References

[1] Soule, R., *et al.*, "Neutronic Studies in Support of Accelerator-driven Systems: The MUSE Experiments in the MASURCA Facility", *Nucl. Sci. Eng.*, 148, 124 (2004).

[2] Gonzalez, E., "The MUSE4 Experimental Results", *Proceedings International Workshop*, Rome, Italy, 21-22 October 2004.

[3] Persson, C., *et al.*, "Yalina Subcritical Assembly: Neutron Kinetic Analysis and Reactivity Determination", *Trans. Am. Nucl. Soc.*, Vol. 92, pp. 259-260 (2005).

[4] Creation of Subcritical Assembly Driven by Proton Accelerator (SAD), ISTC Project 2267 *http://tech-db.istc.ru/istc/sc.nsf/html/projects.htm?open&id=2267*.

[5] Aït Abderrahim, H., P. Baeten, "The GUINEVERE-project at VENUS, Project Status", *ECATS Meeting*, Cadarache, 31.01.2008.

[6] Sjöstrand, N.G., "Measurements on a Subcritical Reactor Using a Pulsed Neutron Source", *Arkiv för Fysik*, 11, 13 (1956).

[7] Ott, K., R. Neuhold, *Introductory Nuclear Reactor Dynamics*, American Nuclear Society (1985).

[8] Merk, B., "An Analytical Solution for a Simple Time Dependent Neutron Transport Problem with External Source", *20th International Conference on Transport Theory*, 22-28 July, Obninsk (2007).

[9] Merk, B., "An Analytical Solution for a Time Dependent Neutron Transport Problem with External Source and Delayed Neutron Production", *Nuclear Science and Engineering*, forthcoming.

[10] Weinberg, A.M., E.P. Wigner, *The Physical Theory of Neutron Chain Reactors*, The University of Chicago Press, Chicago (1958).

[11] Özisik, M.N., B. Vick, "Propagation and Reflection of Thermal Waves in a Finite Medium", *Int. J. Heat Mass Transfer,* Vol. 27, No. 10, 1845-1854 (1984).

[12] Tang, D.W., N. Araki, "The Wave Characteristics of Thermal Conduction in Metallic Films Irradiated by Ultra-short Laser Pulses", *J. Phys. D: Appl. Phys.*, Vol. 29, 2527-2533 (1996).

[13] Duffy, D.G., *Green's Functions with Application*, Chapman & Hall/CRC Boca Raton (2001).

[14] Merk, B.R., D.G. Cacuci, "Multiple Time Expansions for Neutron Kinetics. I: Illustrative Application to the Point-kinetics Model", *Nuclear Science and Engineering*, 151, 184-193 (2005).

[15] Merk, B.R., D.G. Cacuci, "Multiple Time Expansions for Neutron Kinetics. II: Illustrative Application to P1 and P3 Equations", *Nuclear Science and Engineering*, 151, 194-211 (2005).

[16] Meyer, J.E., "Synthesis of Three-dimensional Power Shapes", *2nd International Conference on Peaceful Uses of Atomic Energy*, Geneva, Switzerland, 1-13 September 1958.

Future experiments on minor actinide characteristics using accelerator-driven system in Kyoto University Critical Assembly

Cheol Ho Pyeon, Tsuyoshi Misawa, Hironobu Unesaki, Ken Nakajima, Seiji Shiroya
Nuclear Engineering Science Division, Research Reactor Institute, Kyoto University
Asashiro-nishi, Kumatori-cho, Sennan-gun, Osaka, Japan

Abstract

The accelerator-driven system (ADS) experiments in the Kyoto University Critical Assembly (KUCA) are planned to conduct using 150 MeV protons generated from the Fixed-field Alternating Gradient (FFAG) accelerator. Prior to the ADS with 150 MeV protons, the basic irradiation experiments have been conducted for neutron spectrum measurement using the foil activation method at both a PoP model FFAG accelerator and a synchrotron accelerator. From the results of these basic experiments, it has been concluded that the activation foil of ^{209}Bi is useful for obtaining neutron spectrum information from neutron generation reactions of ^{184}W target for the high-energy protons. And, for the high-energy protons, a comparison of the experiments and the calculations with combination of MCNPX and ENDF/B-VI is found to be a large discrepancy in the reaction rate analyses.

1 Introduction

The Kyoto University Research Reactor Institute (KURRI) is going ahead with a research project [1] on the accelerator-driven system (ADS) using the Fixed-field Alternating Gradient (FFAG) accelerator [2]. FFAG accelerator, which is a synchrotron-type accelerator, was developed at the High Energy Accelerator Research Organization (KEK) of Japan. The goal of the research project is to establish a next-generation neutron source by introducing a synergetic system comprising a research reactor and a particle accelerator, and to demonstrate the basic feasibility of ADS as a next-generation neutron source multiplication system using the Kyoto University Critical Assembly (KUCA) coupled with a newly developed variable energy FFAG accelerator. In ADS experiments, the high-energy neutrons generated at a tungsten (^{184}W) target with 150 MeV proton beam will be injected into a solid-moderated and reflected core (A-core) in thermal neutron field of KUCA.

Prior to the ADS experiments with 150 MeV protons, it is inevitable to evaluate neutronic characteristics of ADS and to establish measurement techniques for several neutronic parameters in ADS. For these purposes, a series of the ADS experiments with 14MeV neutrons [3,4] generated by D-T reactions at a Cockcroft-Walton-type accelerator [5] had been carried out at the KUCA A-core. In these experiments, several neutronic parameters had been measured: neutron multiplication; neutron decay constant; reaction rate distribution; neutron spectrum; subcriticality. The numerical analyses for the experiments had been executed using Monte Carlo calculation code MCNP-4C3 [6] coupling with nuclear data libraries: ENDF/B-VI.2 and JENDL-3.3. Through these analyses, the important and valuable results have been obtained for the neutronic characteristics of ADS. After completing the ADS experiments with the FFAG accelerator, the consequent ADS experiments are planned to add the γ-ray spectrum detection at the target and in the core region, and the power monitoring of the core during beam current change and moving control rods. Moreover, these experiments could be possibly carried out in several neutron spectrum and γ-ray fields using the cores consisting of several kinds of fuel and reflectors; highly enriched uranium, thorium fuel and natural uranium; polyethylene, aluminium, beryllium and graphite.

In this study, for neutron spectrum measurement of the high-energy neutrons, the basic irradiation experiments have been conducted using the foil activation method at both a PoP-type FFAG accelerator of KEK and a synchrotron accelerator of Hospital East of the National Cancer Centre in Japan. Then, the high-energy neutron spectrum over 20 MeV were evaluated using the nuclear reactions of ^{209}Bi(n,xn)$^{210-x}$Bi (x = 3 through 12) in these experiments. The objective of this study is to examine experimentally the neutron spectrum at a target region in a high-energy neutron field using the nuclear reactions of the bismuth (^{209}Bi). The FFAG accelerator, the KUCA A-core configuration and the ADS benchmark problems are presented in Section 2; the results of experiments and analyses by MCNPX [7] with ENDF/B-VI [8] in Section 3, and the summary of the study in Section 4.

2 ADS in KUCA

2.1 FFAG accelerator

The conceptual image of ADS in KURRI is shown in Figure 1. In the ADS with 150 MeV protons, all of ion beta, booster and main accelerator is composed of FFAG accelerators, and maximum power of the KUCA A-core and maximum neutron yield could be 100 W and 1×10^{10}*n*/*s*, respectively, when 150 MeV protons generated from the FFAG accelerator are injected onto ^{184}W target. The main characteristics of the FFAG accelerator are indicated in Table 1. Maximum and average beam currents of the FFAG accelerator are 1 μA and 1 nA, respectively.

2.2 ADS benchmark problems

KUCA is equipped with these following cores coupling several kinds of the fuel and the reflectors:

- polyethylene-moderated and reflected core with highly enriched uranium fuel;
- graphite-moderated and reflected core with thorium fuel;
- (polyethylene + graphite)-moderated and reflected core with (thorium + natural uranium) fuel;
- neutronic decoupling core modelling large size core.

Figure 1: Conceptual image of ADS with the FFAG accelerators in KURRI

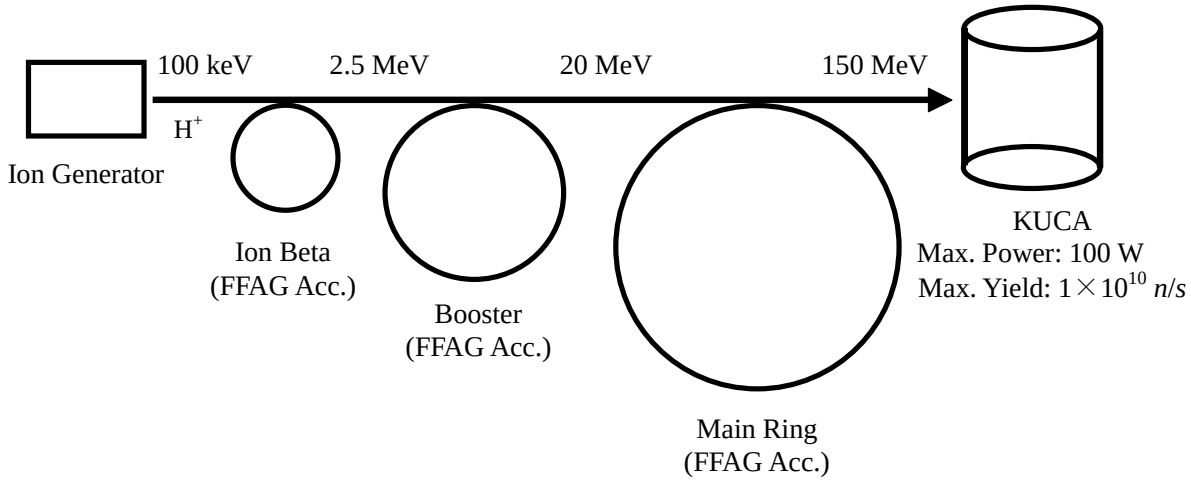

Table 1: Main characteristics of the FFAG accelerator

Number of sectors	12
Proton energy	2.5-150 MeV
Repetition rate	120 Hz
Pulsed width	60 ns
Beam current	1 μA (max.), 1 nA (ave.)
Rf frequency	1.5-4.6 MHz
Field index	7.5
Closed orbit radius	4.4-5.3 m

Figure 2: Top view of configuration of A-core with neutron guide conducted in neutron spectrum experiments

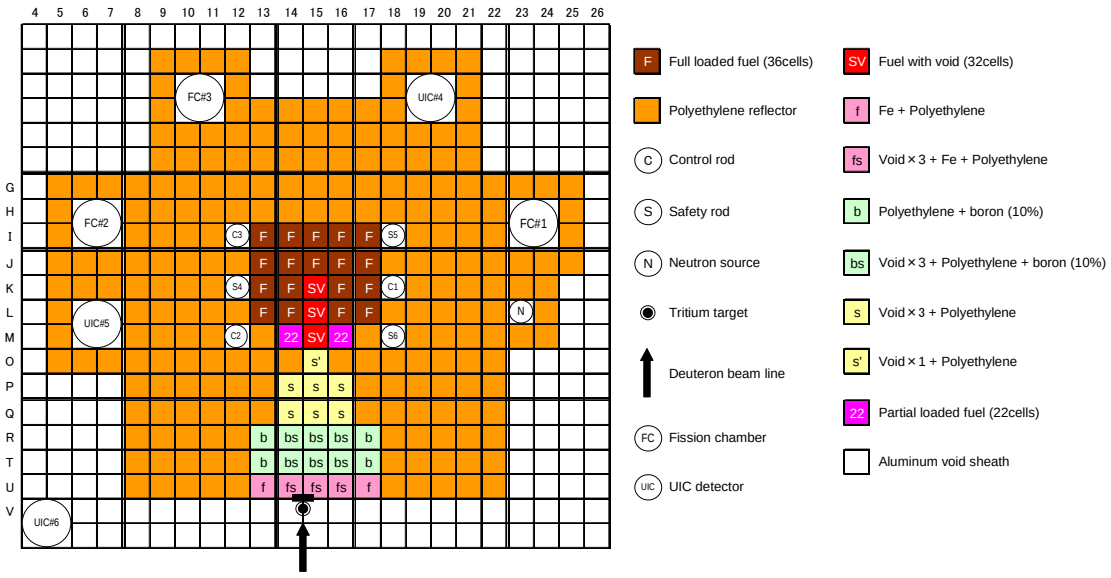

After introducing FFAG accelerator, reactor physics experiments on ADS are planned at a next stage as follows:

- measurement of subcriticality by pulsed neutron method, neutron noise methods and source multiplication method;
- measurement of reaction rate distribution in the core by the foil activation method and optical fibre detection system;
- measurement of neutron spectrum by the foil activation method and organic scintillator;
- evaluation of neutron multiplication characteristics ($M = S/1 - k_{eff}$);
- γ-ray spectrum detection at the target and in the core regions;
- power monitoring of the core in case of beam current change or moving control rods;
- optimisation of the neutron guide installed in the A-core.

Both new experiments and numerical simulations could be conducted for the high-energy neutrons obtained by 150 MeV protons generated from FFAG accelerator, on the basis of the important and valuable information obtained in the ADS experiments with 14 MeV neutrons. Now, several benchmark experiments are opened not only to Japan but also to other countries in the future. On the other hand, these benchmark problems are positioned as basic research for the ADS development and nuclear transmutation technology in co-operation with international collaboration research programme [9] published by the J-PARC project of JAEA.

3 Neutron spectrum experiments

3.1 FFAG accelerator

FFAG accelerator in PoP (proof-of-principle) model had been constructed at KEK on March 2005, and the neutron spectrum experiments were conducted in an irradiation hole shown in Figure 3(a) of FFAG accelerator in PoP model, although high-energy proton beam was not concentrated adequately with a slender due to just commissioning. A specific flange shown in Figure 3(b) setting ^{184}W target, ^{93}Nb and ^{209}Bi was placed in the irradiation hole. In these experiments, ^{209}Bi was utilised for measuring reactions rates, and ^{93}Nb as a normalisation factor of neutron yield generated from ^{184}W target. The size of ^{184}W and ^{209}Bi $50\phi \times 3$ mm^3 for each of them, that of ^{93}Nb $20 \times 20 \times 1$ mm^3. The beam injection onto ^{184}W target was conducted with below 100 MeV of proton energy and 0.4 nA of beam intensity, and in about three hours of irradiation time. The reaction rates were obtained by nuclear reactions of ^{209}Bi covering a wide range of threshold energy about 15 MeV to 90 MeV according to changing the value of *x*. In other words, the neutron spectrum information on this irradiation field can be easily acquired by irradiating ^{209}Bi foil once, especially in high-energy region more than 15 MeV.

The results in measured reaction rates obtained by the proton beam injection are shown in Table 2. From the results in Table 2, it was considered that the high-energy neutrons from about 20 to 50 MeV were generated by the injection of the high-energy protons onto ^{184}W target. As shown in Figure 4, the results of calculated neutron spectrum generated from ^{184}W target were obtained by using MCNPX. From these results, it was inferred that the high-energy protons in about 70 MeV were generated from the FFAG accelerator and was injected onto ^{184}W target. In these neutron spectrum experiments, it was concluded that the neutrons up to 50 MeV can be obtained by about 70 MeV proton beam injection onto ^{184}W target.

Table 2: Measured reaction rates obtained at irradiation hole of the FFAG accelerator

Reaction	Threshold (MeV)	Half-life	Measured reaction rate (1/s/cm^3)
^{209}Bi(n,3n)^{207}Bi	14.42	38.3 y	–
^{209}Bi(n,4n)^{206}Bi	22.55	6.24 d	$(1.51\pm0.01)\times10^{5}$
^{209}Bi(n,5n)^{205}Bi	29.62	15.31 d	$(1.01\pm0.03)\times10^{5}$
^{209}Bi(n,6n)^{204}Bi	38.13	11.22 h	$(2.37\pm0.02)\times10^{4}$
^{209}Bi(n,7n)^{203}Bi	45.37	11.76 h	$(6.35\pm0.16)\times10^{3}$
^{209}Bi(n,8n)^{202}Bi	54.24	1.67 h	$(2.74\pm0.07)\times10^{2}$
^{209}Bi(n,9n)^{201}Bi	61.69	1.77 h	–
^{209}Bi(n,10n)^{200}Bi	70.89	36.45 m	–
^{209}Bi(n,11n)^{199}Bi	78.47	27.12 m	–
^{209}Bi(n,12n)^{198}Bi	87.94	11.85 m	–

Figure 3: Simple image of irradiation hole at FFAG accelerator and flange setting activation foils

(a) Irradiation hole at the FFAG accelerator setting outside beam dump

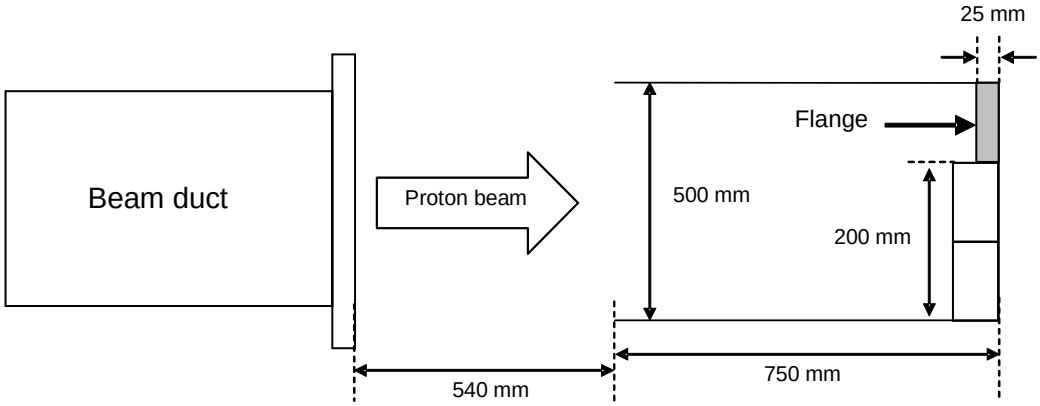

(b) Flange setting activation foils (W, Nb and Bi)

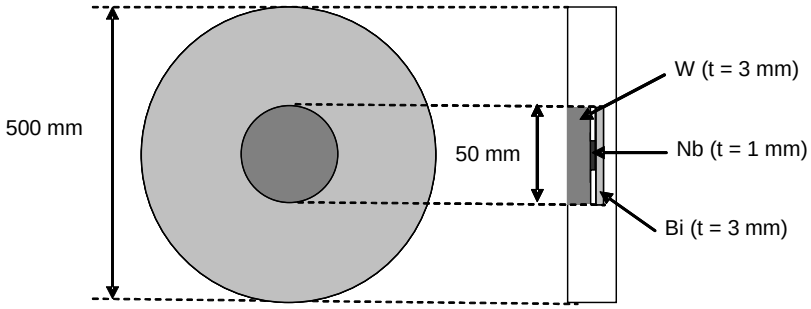

Figure 4: Calculated results of neutron spectrum obtained by MCNPX code

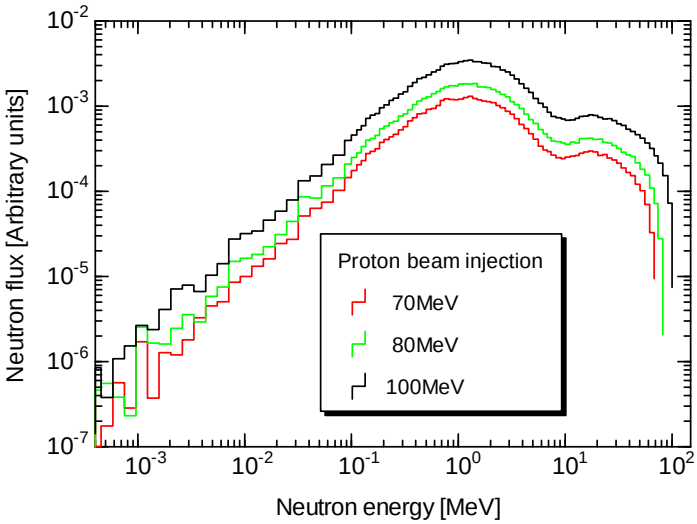

3.2 High-energy proton beam

The neutron spectrum experiments were carried out at an irradiation facility in Hospital East of the National Cancer Centre. 150 MeV proton beam in 0.1 nA intensity was injected onto ^{184}W target. As shown in Figure 5, the experimental setting was equipped with these following materials: ^{184}W target of 50ϕ mm diameter in 3 mm thickness; ^{209}Bi of 50ϕ mm diameter in 21 mm thickness for obtaining the reaction rates; aluminium (Al) plate of 50ϕ mm diameter in 1 mm thickness for normalisation of proton injection; the Gafchromic film for monitoring proton particle profile. ^{184}W target thickness varying according to the proton energy was estimated by both using SRIM code [10] and monitoring the results of Gafchromic films set in both top and bottom sides of the experimental setting. At the synchrotron accelerator, 150 MeV proton beam in 0.1 nA beam current with 2.5 cm beam spot size was injected onto ^{184}W target.

Figure 5: Cross-section of an experimental setting using W target, Bi foil, Al plate and Gafchromic film

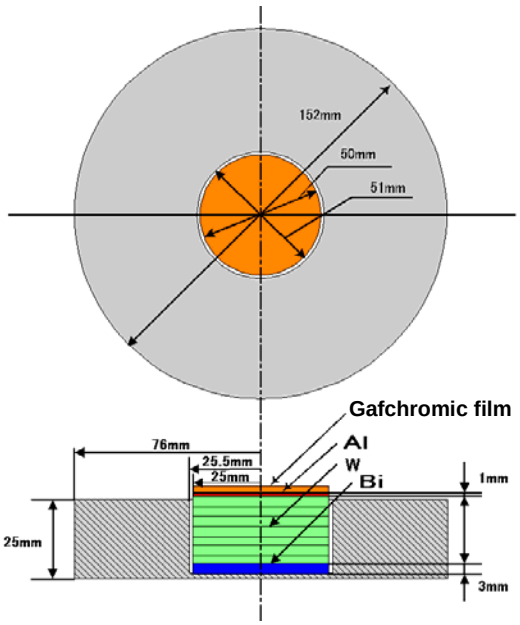

3.3 Measurements and calculations

The high-energy neutron spectrum information can be obtained using the nuclear reactions of ^{209}Bi, and the cross-sections [11] evaluated by the experiments and calculations were shown in Figure 6. In these experiments, 150 MeV proton beams, which can be varied from 100 to 235 MeV at maximum intensity 0.3 mA, was injected onto ^{184}W target, and the γ-ray count was measured using the high purity germanium (Ge) detector for an experimental feasibility study of the measurement technique. Whereas, in MCNPX calculations, the experimental setting was modelled precisely and the reaction rates of ^{209}Bi were numerically estimated. A comparison of measured and calculated reaction rates was conducted for an estimation of the MCNPX calculation precision.

Figure 6: Cross-sections obtained by the experiments

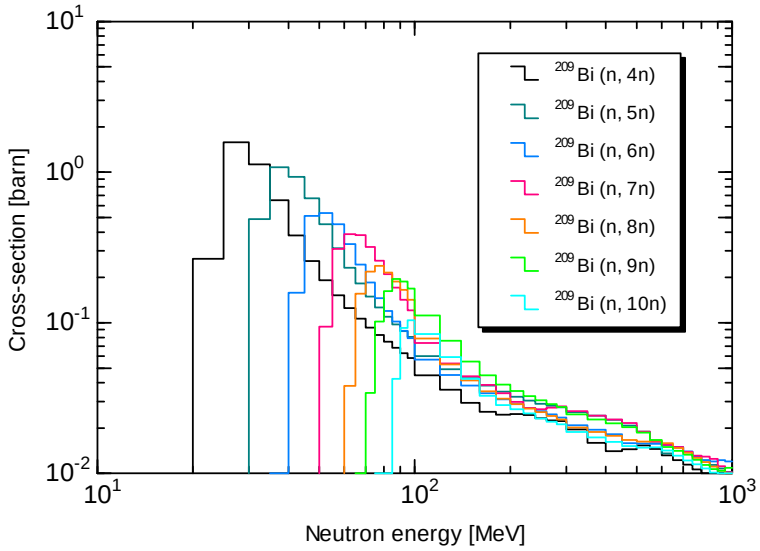

3.3.1 Results and discussion

The experimental results of the reaction rates were obtained by measuring total counts of the peak energy of γ-ray emittance shown in Figure 7, such as ^{209}Bi foil. The saturation activity D_∞ was evaluated by the following equation:

$$D_\infty = \frac{100\lambda T_c C(1+\alpha)}{\varepsilon\left(1-e^{-\lambda T_i}\right)e^{-\lambda T_w}\left(1-e^{-\lambda T_c}\right)} \quad (1)$$

where, λ indicates the decay constant, T_c the measurement counting time, C the counting rate, α an internal conversion coefficient, ε a detection efficiency, T_i the irradiation time, and T_w the waiting time until the start of the measurement after the irradiation. Finally, the reaction rate can be obtained using this saturation activity as seen in Eq. (1).

The result of the γ-ray spectra shown in Figure 7 was in case of ^{209}Bi foil irradiated by the neutrons generated from 150 MeV protons in 0.1 nA intensity. The several nuclear reactions were observed clearly in these experiments.

As shown in Table 3, the results of 150 MeV protons in the comparison of measured and calculated reaction rates by ^{209}Bi(n,xn)$^{210-x}$Bi reactions were observed with a good agreement within about 30% in relative difference of the C/E value except for (n,5n) reaction. In these experiments, the reaction rate of (n,3n) reaction was not found due to no activation caused by its long half-life, including the additional results in 100, 190 and 235 MeV protons. Subsequently, it was considered to show a proton energy dependency in (n,11n) reaction.

Figure 7: Measured γ-ray spectra from Ge detector for ^{209}Bi foil in case of protons of 150 MeV with an intensity of 0.1 nA

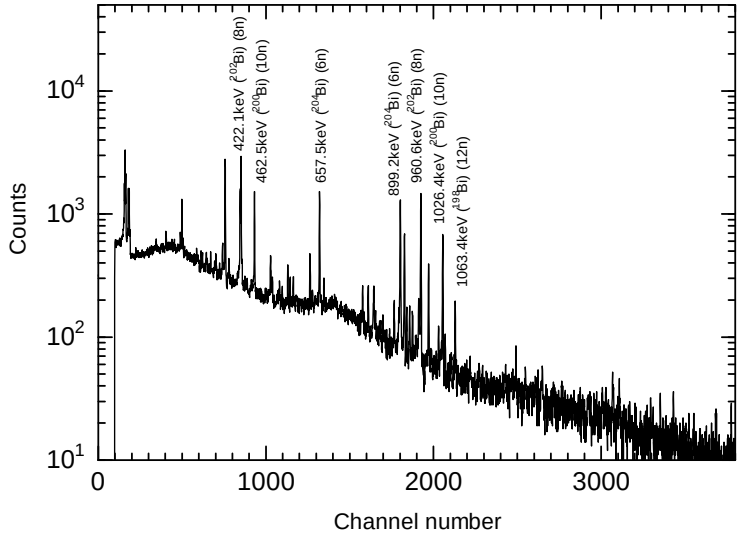

Table 3: C/E values between measured and calculated reaction rates of ^{209}Bi(n,xn)$^{210-x}$Bi reactions (x = 3 to 12) in 100, 150, 190 and 235 MeV protons with 0.1 nA

Reaction	100 [MeV]	150 [MeV]	190 [MeV]	235 [MeV]
^{209}Bi(n,3n)^{207}Bi	—	—	—	—
^{209}Bi(n,4n)^{206}Bi	3.96±0.13	1.32±0.11	1.33±0.02	1.02±0.01
^{209}Bi(n,5n)^{205}Bi	3.29±0.18	2.01±0.19	1.36±0.03	0.84±0.02
^{209}Bi(n,6n)^{204}Bi	2.20±0.06	0.95±0.08	0.90±0.02	0.68±0.01
^{209}Bi(n,7n)^{203}Bi	2.02±0.10	1.11±0.10	1.13±0.02	0.76±0.01
^{209}Bi(n,8n)^{202}Bi	1.00±0.03	1.00±0.12	1.00±0.02	1.00±0.01
^{209}Bi(n,9n)^{201}Bi	0.83±0.09	1.24±0.12	1.21±0.05	1.12±0.08
^{209}Bi(n,10n)^{200}Bi	0.37±0.03	0.95±0.08	1.21±0.03	1.19±0.02
^{209}Bi(n,11n)^{199}Bi	—	—	1.53±0.07	1.26±0.04
^{209}Bi(n,12n)^{198}Bi	—	0.98±0.09	1.34±0.10	1.24±0.08

4 Summary

Prior to the ADS with 150 MeV protons, the basic irradiation experiments have been conducted for neutron spectrum measurement using the foil activation method at both a PoP-type FFAG accelerator and a synchrotron accelerator. From the results of these experiments, it was concluded that the activation foil of ^{209}Bi was useful for obtaining neutron spectrum information using the neutron generation reactions of ^{184}W target for the high-energy protons. And, for the high-energy protons, a comparison of the experiments and the calculations with combination of MCNPX and ENDF/B-VI is found to be a little discrepancy in the reaction rate analyses.

In the future, it is expected that the basic research activity of ADS could be progressed through the ADS with 150 MeV protons generated from the FFAG accelerator. After completing the examinations of FFAG accelerator, the consequent ADS experiments with 150 MeV protons are planned to carry out at KUCA, including γ-ray spectrum detection at the target and in the core region, power monitoring of the core during beam current change and moving control rods. Moreover, on the basis of the integral measurements on minor actinides (MA) of ^{237}Np and ^{241}Am, future experiments could be possibly carried out at KUCA using the back-to-back chamber for the investigation of MA characteristics in the ADS with 150 MeV protons.

Acknowledgements

This work was supported by the Ministry of Education, Culture, Sports, Science and Technology of Japan within the task of "Research and Development for an Accelerator-driven Subcritical System Using an FFAG Accelerator".

The authors extend special thanks to Professor Teiji Nishio of University of Tokyo and all the technical staff of Hospital East of the National Cancer Centre in Japan, and to Mr. Hiroshi Shiga of Kyoto University for his contribution in executing the computational procedures.

References

[1] Shiroya, S., H. Unesaki, Y. Kawase, H. Moriyama, M. Inoue, "Accelerator Driven Subcritical System as A Future Neutron Source in Kyoto University Research Reactor Institute (KURRI) – Basic Study on Neutron Multiplication in the Accelerator Driven Subcritical Reactor", *Prog. Nucl. Energy*, 37, 357 (2000).

[2] Machida, S., "Design and Particle Tracking of FFAG", *Nucl. Instrum. Methods A*, 503, 318 (2003).

[3] Pyeon, C.H., Y. Hirano, T. Misawa, H. Unesaki, C. Ichihara, T. Iwasaki, S. Shiroya, "Preliminary Experiments on Accelerator-driven Subcritical Reactor with Pulsed Neutron Generator in Kyoto University Critical Assembly", *J. Nucl. Sci. Technol.*, 44, 1368 (2007).

[4] Pyeon, C.H., M. Hervault, T. Misawa, H. Unesaki, T. Iwasaki, S. Shiroya, "Static and Kinetic Experiments on Accelerator-driven System in Kyoto University Critical Assembly", *J. Nucl. Sci. Technol.*, 45 (2008).

[5] Ichihara, C., *et al.*, *Characteristics of KUCA Pulsed Neutron Generator*, Kyoto University Research Reactor Institute Technical Report, KURRI-TR-240 (1983) (in Japanese).

[6] Briesmeister, J.F. (Ed.), *MCNP – A General Monte Carlo N-Particle Transport Code, Version 4C*, Los Alamos National Laboratory, Report LA-13709-M (2000).

[7] Waters, L.W. (Ed.), *MCNPX User's Manual Version 2.3.0*, Los Alamos National Laboratory, Report LA-UR-02-2607 (2002).

[8] Rose, P.F., *ENDF-201, ENDF/B-VI Summary Documentation*, BNL-NCS-17541, 4th Edition (1991).

[9] JAEA web page, *http://j-parc.jp/documents/pdf/loi/Call_for_pre_LOI.pdf*.

[10] Eiegler, J.F., *et al.*, *The Stopping and Range of Ions in Matter*, Pergamon Press, New York (1985).

[11] Kim, E., T. Nakamura, A. Konno, *et al.*, "Measurements of Neutron Spallation Cross Sections of ^{12}C and ^{209}Bi in the 20- to 150-MeV Energy Range", *Nucl. Sci. Eng.*, 129, 209 (1998).

Determination of ^{241}Am cross-sections

C. Sage, A. Borella, S. Kopecky, A. Plompen, P. Rullhusen,
P. Schillebeeckx, V. Semkova, P. Siegler
European Commission, Joint Research Centre
Institute for Reference Materials and Measurements
Geel, Belgium

Abstract

Cross-sections of neutron-induced reactions on ^{241}Am have been measured at the nuclear facilities of JRC-IRMM. Transmission measurements have been carried out with high-energy resolution at the GELINA time-of-flight facility. Capture experiments at GELINA are in progress. Although these measurements are still in progress, some preliminary results are presented. Cross-sections for the ^{241}Am(n,2n)^{240}Am reaction have been performed at the Van de Graaff accelerator of JRC-IRMM using the activation technique.

Introduction

To predict reliably the behaviour of reactor cores while burning minor actinides, accurate data concerning cross-sections are a prerequisite. Unfortunately, the present evaluated data files of ^{241}Am do not fulfil these stringent requirements. To address two of the problems encountered in these files, an experimental programme has been developed.

The first problem that should be addressed concerns the resonance parameters of the low-lying americium resonances, as it has been observed that the resonance integral as calculated from the resonance parameters of the evaluated data files is smaller than the value determined by integral measurements. The evaluations for the lowest resonances are based on three measurements (Adamchuck [1], Belanova [2,3], Slaughter [4]). As already observed and reported by O. Bouland [5], the agreement for the lowest resonances between Adamchuck, *et al.* and Belanova, *et al.* are satisfactory, neglecting a small shift in the energies of the lowest resonance, but the results by Slaughter, *et al.* are different [see Figure 1(a)]. The peak cross-sections of the resonances are approximately 30% higher than for the two other measurements. The cross-sections as suggested in the evaluation are typically somewhere in between those two curves. To explain these rather large discrepancies, the influence of the sample properties when powder materials are used is under investigation. Therefore, a set of transmission and capture measurements using a novel sample type have been performed at GELINA, the white neutron source at IRMM.

Another important indication of problems with earlier measurements is the inconsistency that the total cross-section in the thermal range – essentially the result of Belanova and Adamchuk – is about 50 b less than the present best value for the capture cross-section.

The second point that has caught our attention is the ^{241}Am(n,2n)^{240}Am cross-section. Firstly, in the energy range between 8 and 16 MeV significant differences between the different evaluations (JEFF-3.1, BROND-2.2 and ENDF/B-VII) are observed [see Figure 1(b)]. The main reason is the small number of experimental data points – which are even disagreeing – in this energy range. Moreover, at energies above approximately 15 MeV no experimental data are available. To address this problem, measurements were performed at the 7 MeV Van de Graaff accelerator at JRC-IRMM using the activation technique.

Figure 1: (a) Previous experimental total cross-section data compared to evaluations, (b) previous experimental ^{241}Am(n,2n)^{240}Am cross-section and evaluation

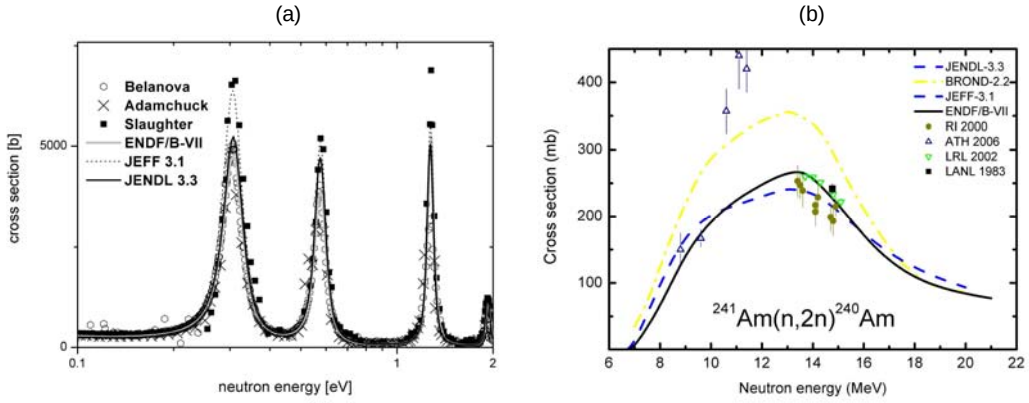

Experiments

The transmission and capture experiments were performed at GELINA, the white neutron source at the Institute for Reference Materials and Measurements. GELINA is a linear electron accelerator that accelerates electrons up to 150 MeV and has a peak current of 12 A. Electron pulses have a duration of approximately 1 ns, thanks to a post-acceleration pulse-compression magnet. The repetition rate can be varied between 1 and 800 Hz. The electrons strike a depleted uranium target, which is cooled by

mercury. The electrons produce bremsstrahlung and subsequently neutrons, with energies of a few MeV. For moderating the neutrons, two beryllium containers filled with water are mounted above and below the neutron production target. The dimensions of the moderators are approximately $10 \times 10 \times 4$ cm. The moderator thickness of 4 cm predominantly determines the time resolution function of the neutron production. By using different collimation conditions, experiments can either use a fast or a moderated neutron spectrum. Up to 12 experiments can be performed simultaneously at flight paths that lead radially from the neutron production target. Flight path lengths between 10 and 400 m can be chosen, depending on the required energy resolution. For monitoring the neutron flux, BF_3 counters are embedded in the ceiling of the target hall.

To derive the transmission and the capture yields from the registered data the software package AGS [6] was used. This code performs the most important corrections, such as dead-time correction, background subtraction, etc., with a full propagation of the covariance matrix, starting with the statistical uncertainties of the counting statistics.

The background is estimated with the black resonance technique, *i.e.* filters are inserted into the beam, which remove all the neutrons at one given energy. Examples of filter materials are W, Cs, Mo, Au. When using this technique it should always be kept in mind that the insertion of any filter will alter the beam condition and consequently the background. Therefore, the black resonance filters were kept in the beam while the experiment was performed, or the effect of the filter on the background was calculated and corrected.

Transmission measurements

The transmission measurements have been performed at flight path No. 2 of GELINA, a flight path that views the moderator at an angle of 9°. The chosen flight path length was 26.45 m. The beam diameter was limited to approximately 1.5 cm, using a combination of Li carbonate, copper and nickel collimators. The sample was positioned at a distance of approximately 10 m halfway between the neutron target and the detector system. Filters to reduce the intensity of the gamma-flash as well as black resonance filters for estimating the background could be inserted close to the sample position. For neutron detection a 0.5″ thick lithium-glass scintillator was employed, with a diameter of 4 inch viewed by two photomultiplier tubes (EMI9823QKB). In order to separate a valid neutron event from the photomultiplier noise, a coincidence between the signals of both tubes was imposed. An in-house built fast-timing digitiser with a time resolution of 0.5 ns was used for determining the neutron time-of-flight. The time-of-flight data are recorded in histogram mode. To reduce the impact of a variation of the neutron flux on the measured transmission, measurements of the sample and open beam were cycled every 20 minutes.

Since the existing experimental data [1-4] show large discrepancies in the transmission values, one goal of the present measurements was to improve the data by using an improved sample type over the powder based samples from the past. As has been shown in a transmission measurement for ^{240}Pu and ^{242}Pu [7] the structure and especially the grain size of powder based oxide samples can be responsible for a major deviation from the observed resonance shape when compared to literature. Inhomogeneities and grain size distributions have been modelled to describe an overestimation of the capture width and an underestimation of the neutron width, thus resulting in an underestimation of the capture cross-section. To overcome this problem in the present experiments, a sample based on an Y_2O_3 matrix was infiltrated with 325 mg ^{241}Am as oxide providing an equal distribution of Am over the whole sample size.

The transmission of the sample was determined and analysed using the resonance shape analysis code Refit [8]. In Figure 2 the results of such a shape analysis is compared to the transmission as determined with the resonance parameters given in ENDF, JEFF and JENDL. All three evaluations underestimate significantly the cross-sections. As shown in Figure 3 our observed transmission data are in good agreement with transmission data derived from the previous results of Slaughter, *et al.* [4], but seem to disagree with Adamchuck, *et al.* [1] and Belanova, *et al.* [2]. On the other hand, for the energies of the resonances the agreement seems to be better with Belanova, *et al.* [2]. Final results will only be obtained after a simultaneous analysis of the transmission and capture data.

Figure 2: Experimental transmission data compared to different evaluations

(a) First resonance; (b) Analysed region from 0.1 to 20 eV

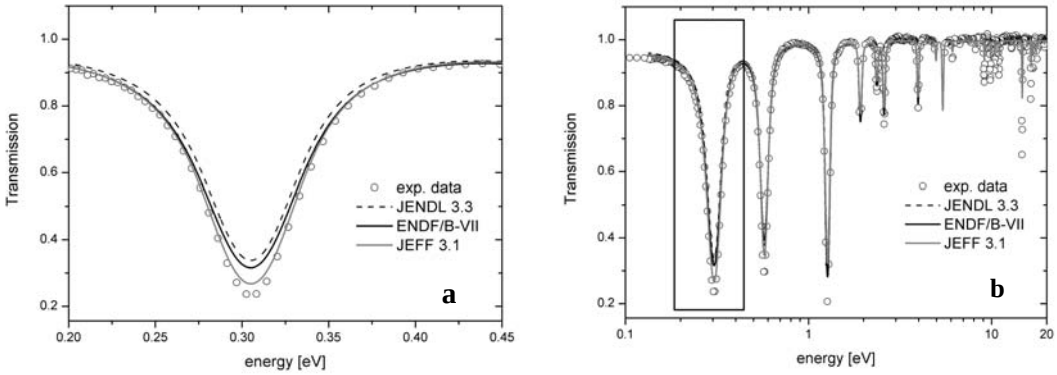

Figure 3: Comparison of IRMM transmission data with values derived from previous experiments

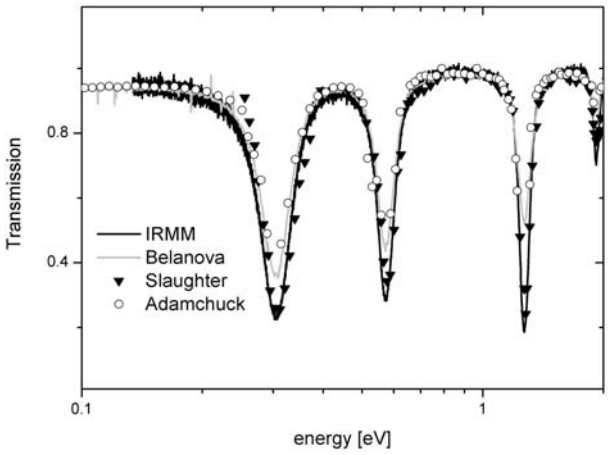

Capture measurements

The first test experiments for determining the capture yield of americium were performed at a flight path length of 10 m with the beam diameter at the sample station reduced to approximately 7.45 cm using Li carbonate plus resin, copper and lead collimators. As for the transmission, the measurement station was air conditioned to keep the sample at a constant temperature and to minimise a drift of the electronics.

The detection of the photons that were produced in the capture event was accomplished by two cylindrical C_6D_6 detectors (NE230). These detectors were mounted at an angle of 125° to reduce the effects caused by the anisotropy of the dipole radiation (c.f. Figure 4). To minimise the detection of scattered neutrons in the detector system, the scintillators were mounted directly on photomultipliers with quartz windows. The pulse height weighing technique was used to create a detector response proportional to the energy of the registered gamma. A description of the method and of the calculation of the weighting function can be found in Ref. [9].

The americium sample was shielded from the detectors by a cylinder with an inner diameter of approximately 13 cm and a length of 20 cm, which was produced of antimony-free lead and had a thickness of approximately 1 cm. This shielding eliminated the 60 keV line of the decay of ^{241}Am and reduced considerably the intensity of a large number of weaker but more energetic transitions. Such a shield was essential for reducing the time-independent background, as otherwise a good sensitivity and an accurate dead-time correction could not have been guaranteed.

Figure 4: Experimental set-up for the capture measurements

The flux shape was determined with a Frisch gridded ^{10}B ionisation chamber which was operated with a continuous flow of an argon (90%) and methane (10%) mixture (P10). The boron sample itself consisted of approximately 1.25 10^{-5} atoms/barn of ^{10}B evaporated on a 30 µm Al backing.

The amplitude and the time-of-flight of each event were recorded in list-mode for off-line data reduction. This allows for a very careful monitoring of the stability of the detection system. The linearity of the scintillator system was checked periodically, every weekend while the accelerator was shut down, by measuring the 661.7 keV line of the ^{133}Cs decay and the 6.13 MeV line from a ^{238}Pu+^{13}C source. Furthermore, the 2.2 MeV gamma line from the H neutron capture in the moderator, a permanently present background in our measurements, was used to verify the stability.

For the capture measurements the first tests were successful. Figure 5 displays data taken within two days. The signal-to-background ratio in the resonance region is sufficiently high to allow for a reliable determination of the capture yield. Therefore, further experiments to reduce the statistical uncertainty and for a better determination of the induced background are planned for the second half of September 2008.

Figure 5: First capture measurements taken within two days at GELINA

(a) With neutron beam; (b) Without neutron beam

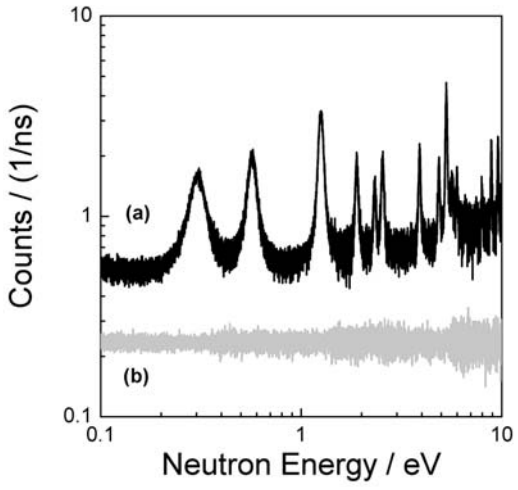

Activation measurements

A determination of the ^{241}Am(n,2n)^{240}Am reaction cross-section is very difficult, as a neutron multiplicity experiment has to exclude neutrons produced in fission events and a measurement of prompt gammas would lead to an underestimation of the cross-section due to internal conversion and the impossibility to observe the direct population of the ground state. The activation method avoids these problems but is applicable to only a few actinides on account of constraints imposed by the natural activity and availability of sample material. As a result relatively few actinide (n,2n) data are known well enough to provide good tests for model estimates.

Three sets of irradiations were performed. The first set used quasi mono-energetic neutrons with energies of 8.8 and 9.4 MeV produced via the ^{2}H(d,n)^{3}He on a gas target. The two other experiments, determining for the first time the reaction cross-section above 15 MeV, used neutrons with energies between 16.2 and 20.7 MeV produced via the ^{3}H(d,n)^{4}He reaction. During the irradiation a long counter was used to record the time profile of the neutron flux to allow for a correction of the fluctuations.

The neutron flux as a function of deuteron energy and detection angle was calculated using the program EnergySet, and the fluence rate was determined by the reaction ^{27}Al(n,α)^{24}Na. Furthermore, to control the neutron energy distribution, various dosimetry reactions with different energy thresholds, such as ^{115}In(n,n′)^{115}In, ^{58}Ni(n,p)^{58}Co, and ^{27}Al(n,p)^{27}Mg were used. The samples contained between 30 and 40 mg of ^{241}Am oxide that had been infiltrated into an Al_2O_3 matrix.

After the irradiation, the induced activity was measured off-line using a high-purity germanium detector. For the data acquisition the Maestro system from EG&G Ortec was employed and for the analysis of the gamma spectra the software package Genie-2000. The decay data used for the data analysis were taken from the Nuclear Data Sheets. A shielding had to be used to reduce the 60 keV gamma line from the ^{241}Am decay in order to limit the dead-time of the system to less than 10%. The efficiency of the detection system was determined by a Monte Carlo simulation using the MCNP5 code. The cross-sections were extracted using the formulas for activation analysis, including corrections for the time-dependent neutron flux, flux contributions from neutrons with lower energies and geometrical effects in the irradiation and measurements.

As depicted in Figure 6 the so derived cross-section data are within the uncertainties in agreement with the results obtained at TUNL in 2007 [10]. Concerning the results from Athens [11], the data agree at low energies (below 10 MeV) whereas in the range of 10-15 MeV a significant difference can be observed. Over the whole energy range our experimental data agree rather well with the ENDF/B-VII evaluation. The agreement with the model calculation of in particular ENDF/B-VII and to a somewhat lesser extent JEFF-3.1 is remarkable given the fact that these were based on knowledge about the data at 14 MeV only and are otherwise based on physical arguments and data for the fission process.

Figure 6: Experimental ^{241}Am(n,2n) cross-sections obtained at IRMM compared to previous data and evaluations

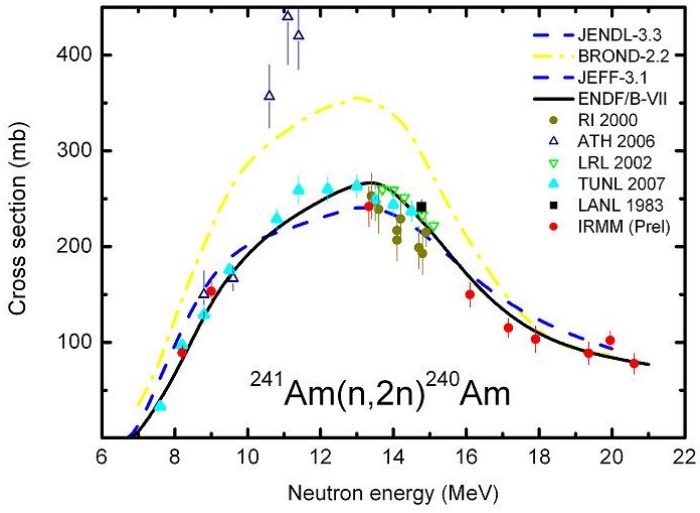

Conclusions

To address existing problems with integral data and the evaluated data files for ^{241}Am a measurement campaign at JRC-IRMM has been started including transmission, capture and activation experiments. A novel type of samples based on AmO_2 infiltration in a Y_2O_3 matrix was used. Results of the transmission experiments for the first resonances show an underestimation of the cross-section by the various evaluations. First tests with capture measurements have been successfully performed. Further experiments are ongoing to reduce the statistical uncertainties. Once both types of measurements are completed, the results of a detailed resonance shape analysis can be used as a basis for a new evaluation.

Three campaigns of activation measurements for the ^{241}Am(n,2n) reaction were performed at the Van de Graaff accelerator. The results are compared to existing data and recent evaluations. The consistency with other recent experimental data was shown for neutron energies below 14 MeV. The present work is the first to report results above 14 MeV. A remarkable agreement was obtained with the model calculations of ENDF/B-VII for this reaction. It may be noted that these calculations were performed prior to the experimental works of Tonchev, *et al.* [10] and that reported here.

References

[1] Adamchuck, Yu.V., V.F. Gerasimov, B.V. Efimov, *et al.*, *Proceedings of the First UN Conference on the Peaceful Uses of Atomic Energy*, Geneva, Switzerland, p. 216, p. 259 (1955).

[2] Belanova, T.S., A.G. Kolesov, V.M. Nikolaev, *et al.*, "Parameters of the Neutron Resonances of ^{241}Am in the Energy Range from 8 to 30 eV", *Atom. Ener.*, 38, 33 (1974).

[3] Kalebin, S., V.S. Artamonov, R.N. Ivanov, *et al.*, "Total Neutron Cross-section and Neutron Resonance Parameters of ^{241}Am in the Energy Range 0.004-30 eV", *Atom. Ener.*, 40, 373 (1976).

[4] Slaughter, G.G., J.A. Harvey, R.C. Block, ORNL Report 3085, p. 42 (1961).

[5] Bouland, O., *Motivation for New ^{241}Am Measurements*, JEF/DOC-931.

[6] Bastian, C., A. Borella, F. Gunsing, J. Heyse, S. Kopecky, G. Noguerre, P. Siegler, P. Schillebeeckx, "AGS – A Computer Code for Uncertainty Propagation in Time-of-flight Cross-section Data", *American Nuclear Society's Topical Meeting on Reactor Physics (PHYSOR-2006)*, Volume 2006.

[7] Kopecky, S., P. Siegler, A. Moens, "Low Energy Transmission Measurements of ^{240,242}Pu at GELINA and Their Impact on the Capture Width", *Proceedings of the International Conference on Nuclear Data for Science and Technology*, Nice, France, Vol. 1, p. 623 (2007).

[8] Moxon, M.C., T.C. Ware, C.J. Dean, *REFIT-2007, A Least-square Fitting Program for Resonance Analysis of Neutron Transmission, Capture, Fission and Scattering Data*, UKNSF(2006)P216 (2007).

[9] Borella, A., G. Aerts, F. Gunsing, M. Moxon, P. Schillebeeckx, R. Wynants, "The Use of C_6D_6 Detectors for Neutron Induced Capture Cross-section Measurements in the Resonance Region", *Nucl. Instr. Methods*, 577, 626 (2007).

[10] Tonchev, A., C.T. Angell, M. Boswell, *et al.*, "Measurement of the ^{241}Am(n,2n) Reaction Cross-section from 7.6 MeV to 14.5 MeV", *Phys. Rev. C*, 77, 054610 (2008).

[11] Perdikakis, G., C.T. Papadopoulos, R. Vlastou, A. Lagoyannis, A. Spyrou, M. Kokkoris, S. Galanopoulos, N. Patronis, D. Karamanis, Ch. Zarkadas, G. Kalyva, S. Kossionides, "Measurement of the ^{241}Am(n,2n) Reaction Cross-section Using the Activation Method", *Phys. Rev. C*, 73, 067601 (2006).

Continuous-energy cross-section library based on JENDL High Energy File 2007

Toshinobu Sasa, Takanori Sugawara, Tokio Fukahori, Kazuaki Kosako*
Japan Atomic Energy Agency, Japan
*Shimizu Corporation, Japan

Abstract

The latest version of JENDL High Energy File (JENDL/HE-2007) was released in December 2007. The file includes the reaction cross-section of proton and neutron below 3 GeV. One hundred six (106) nuclides for spallation target, neutron moderator, structural material and major/minor actinides are stored to simulate accelerator application such as spallation neutron source and accelerator-driven system. A NJOY-99.251 code was modified to produce a continuous-energy cross-section library for the MCNPX code system from JENDL/HE-2007 to represent various particle release reactions with detailed emitted particle angular distribution. Higher temperature libraries were also produced to simulate reactor systems accurately. Several test calculations were done with typical fast reactor and accelerator-driven transmutation system and good agreement was observed for the k-effective values compared with existing JENDL-3.3 based cross-section library.

Introduction

Requirements for the high energy particle transport analysis with evaluated nuclear data library are increased with the advancement of accelerator applications such as an accelerator-driven system, a spallation neutron source, a radiation therapy, and so on. In actual situation, the analysis related to the above mentioned applications and utilities must use several calculation codes based on different physical analysis schemes. It is desirable to perform the analyses with a consistent and systematic method.

Considering such requirements, evaluation of high energy nuclear data has been performed world wide. In the United States, LA150 cross-section library [1] was released and widely applied for the calculations using MCNPX code [2]. Other countries in Europe and Asia also promote evaluation of high energy reaction cross-sections. In Japan, the first version of JENDL High Energy File (JENDL/HE-2004) [3] was released in March 2004. The library includes neutron- and proton-induced reaction data for 66 nuclides by ENDF-6 format in the energy range from 10^{-5} eV to 3 GeV. The draft version of cross-section library for MCNPX (FSXJHE1) was built from selected 59 nuclides stored in JENDL/HE-2004. Reflecting the feedback information through the benchmark analyses using the FSXJHE1 library, the revised JENDL High Energy File (JENDL/HE-2007) [4] was compiled in December 2007. The file stores nuclear data for 106 nuclides adding newly evaluated 40 nuclides including several minor actinides as listed in Table 1. At this moment, JENDL/HE-2007 is the largest nuclear data file in terms of the number of stored nuclides and the coverage of incident particle energy range. Upcoming final version of JENDL High Energy File is planned to include 132 nuclides up to curium isotopes.

In this paper, the structure and contents of the continuous energy cross-section library FXJH7 series produced from JENDL/HE-2007 and test calculations applying FXJH7 series library are summarised.

Table 1: List of nuclides to be stored in JENDL High Energy File

1st priority (39)	^{1}H, ^{12}C, ^{14}N, ^{16}O, ^{27}Al, ^{50,52,53,54}Cr, ^{54,56,57,58}Fe, ^{58,60,61,62,64}Ni, ^{63,65}Cu, ^{180,182,183,184,186}W, ^{196,198,199,200,201,202,204}Hg, *^{204,206,207,208}Pb, ^{209}Bi, ^{235,238}U*
2nd priority (43)	*^{9}Be,* ^{10,11}B, ^{24,25,26}Mg, ^{28,29,30}Si, ^{39,41}K, ^{40,42,43,44,46,48}Ca, ^{46,47,48,49,50}Ti, ^{51}V, ^{55}Mn, ^{59}Co, ^{90,91,92,94,96}Zr, ^{93}Nb, *^{92,94,95,96,97,98,100}Mo, ^{238,239,240,241,242}Pu*
3rd priority (40)	^{2}H, ^{6,7}Li, ^{13}C, *^{19}F, ^{23}Na, ^{35,37}Cl, ^{35,38,40}Ar,* ^{64,66,67,68,70}Zn, *^{69,71}Ga,* ^{70,72,73,74,76}Ge, *^{75}As, ^{89}Y, ^{181}Ta, ^{197}Au,* ^{232}Th, ^{233,234,236}U, *^{237}Np, ^{241,242,242m,243}Am,* ^{243,244,245,246}Cm
4th priority (10)	^{15}N, ^{18}O, ^{74,76,77,78,80,82}Se, ^{113,115}In

Released in 2004 (66 nucl.), *release in 2007 (103 nucl.),* released after 2007.

Structure of JENDL High Energy File 2007

As experimental cross-section data at high energy range are limited, several kinds of evaluation codes were used together with experimental data to construct JENDL/HE-2007. The structure of the JENDL/HE-2007 file is briefly summarised.

Neutron-induced reaction

Neutron-induced reaction data can be divided into three energy ranges. In the energy range from 10^{-5} eV to 20 MeV, data is taken from JENDL-3.3 [6]. The energy range from 20 MeV to E_i MeV, data is evaluated by combining experimental data and calculated/theoretical values. The E_i value for each nuclide is different from each other and set in the range from 150 to 250 MeV. The energy range above E_i MeV (up to 3 GeV), evaluation was done by calculation. It is noted that the same data as in JENDL-3.3 are stored for carbon and vanadium isotopes below 20 MeV because these nuclides are treated as natural elements in JENDL-3.3.

Proton-induced reaction

The proton incidence file can be divided into two energy ranges; from E_1 MeV to E_i MeV and E_i MeV to 3 GeV. In the lower energy range, evaluation is performed by combining experimental data and

calculated/theoretical values. Evaluation in the other energy range is done by calculation. The values of E_1 and E_i are set according to the structure of each individual nuclides. E_i is taken in the energy range from 150 to 250 MeV. E_1 is set to a lower energy boundary and in some cases, it corresponds to the threshold energy such as 5 MeV for ^{12}C, 1 MeV for ^{56}Fe and ^{208}Pb, etc.

Secondary particle production cross-sections (MT=201 to 207)

For the seven kinds of secondary particle production cross-sections (neutron, gamma, proton, deuteron, triton, ^{3}He and alpha), the JAERI/BNL format, which uses MT=201 to 207 to store them respectively, is adopted as a standard of JENDL/HE file. The LANL format is used to store seven reactions together with special identifier called ZAP in MT=5, which corresponds to MT=201 to 207 in the JAERI/BNL format. Because NJOY has been developed and maintained by Los Alamos National Laboratory, the format which can be processed by NJOY99 is only the LANL format with ZAP identifier. The particle production cross-section is given above 20 MeV for neutron and whole energy range for proton in the JENDL/HE-2007 file. To process these data correctly by NJOY99, a pre-processing program which converts the JAERI/BNL format to the LANL format was prepared and applied.

Pion production cross-sections (MT=208 to 210)

Pion production cross-sections are stored with the assignments of MT=208 to 210 in the JENDL/HE-2007 file. The data for pi-plus, pi-zero and pi-minus are assigned to MT=208, 209 and 210 respectively. The threshold energy of pion production cross-section is set around 150 MeV. However, these data are not included in the present FXJH7 series library.

Fission reaction

In JENDL-3.3, fission cross-section (MT=3/MT=18) is provided to the nuclides above thorium (Z=90). Considering high energy fission reaction, it is convenient to store the fission cross-sections of the nuclides above tungsten (Z=74) in the JENDL/HE-2007 file. Fission cross-section and emitted neutron information (MF=6/MT=18) are provided to neutron- and proton-induced reaction. The number of emitted neutrons (nu-value, MF=1/MT=452) is supplied for neutron-induced fission reaction only.

Treatment of co-ordinate system

As for co-ordinate system of energy-angular distribution for secondary particle production, the evaluation code GNASH [7] adopts the centre-of-mass system whereas another evaluation code JAM uses the laboratory system. Because the co-ordinate system must be unique in current ENDF-6 format, the centre-of-mass system (LAW=1/LANG=2) had been converted into the laboratory system (LAW=7) in JENDL/HE-2007. However, gamma production data are stored with the centre-of-mass system.

Construction of cross-section library for MCNP/MCNPX

To produce cross-section library in the ACE format, which is the format for continuous energy cross-section library specialised to MCNP and MCNPX, the NJOY code is preferable. Several modifications to the modules in latest NJOY99 (Version 99.259, distributed in November 2007) such as NJOY, RECONR, BROADR, HEATR, THERMR, MODER, ACER, and PURR have been applied to process the JENDL/HE-2007 file. Using modified NJOY99.295, FXJH7 cross-section libraries were constructed. FXJH7 libraries are applicable to MCNP5 [8] and MCNPX2.5 or later versions. Other older versions of MCNP or MCNPX do not work correctly with FXJH7 libraries because of newly added function such as: *i)* existence of probability table for unresolved resonance range (ptable); *ii)* adoption of cumulative angular distribution tables based on newfor=1 format; *iii)* application of the new sampling method for charged particle production.

Neutron-induced library

The flow of the processing modules using unresolved resonance parameter is MODER-RECONR-BROADR-HEATR-THERMR-PURR-ACER. In the case of nuclide with no unresolved resonance parameters,

process by PURR module is neglected. The basic condition of data processing by NJOY is summarised as follows:

Precision of pointwise cross-section	0.1%
Temperatures of cross-section	20°C (293.16 K, 2.526×10^{-8}MeV) 300°C (573.16 K) 500°C (773.16 K)
Upper boundary of thermal energy range	4.6 eV
Treatment of inelastic scattering in thermal energy range	Free-gas model
Gamma production data format	Detailed format
Unresolved resonance parameter table	Yes (sigma-zero = 10^{10}, 10^{4}, 10^{3}, 100, 30, 10, 3, 1, 0.1, 10^{-5}), table length = 20 (resonance ladders = 1 000)
newfor option	2 (low67 format)
KERMA calculation method	Energy Balance Method (default) Kinematics Method (^{42,46,48}Ca, ^{47}Ti, ^{92,94,95,96,97,98,100}Mo, ^{181}Ta, ^{182,183,184,186}W, ^{206,207208}Pb, ^{209}Bi)

Using the above condition, three FXJH7 libraries were constructed. The libraries processed with different temperatures, 20°C, 300°C and 500°C are named as FXJH70N1, FXJH71N1 and FXJH72N1, respectively. The ZAID suffix number of each library is 83c, 85c and 87c for ground state nuclides and 84c, 86c and 88c for metastable state nuclide (^{242m}Am).

Proton-induced library

Flow of the processing modules is MODER-RECONR-ACER. The basic conditions for cross-section processing are as follows:

Precision of pointwise cross-section	0.1%
Temperature of cross-section	0 ºK (0 MeV)
Gamma production data format	Detailed format
newfor option	2 (low67 format)

Using this processing condition, FXJH70H1 library for fixed temperature of 0 K was constructed. Suffix of ZAID for FXJH70H1 is 83 h for ground state nuclides and 84 h for metastable nuclide (^{242m}Am only). To keep consistency with neutron cross-section libraries, FXJH71H1 (ZAID suffix = 85 h and 86 h) and FXJH72H1 (ZAID suffix = 87 h and 88 h) were prepared using the same data as FXJH70H1.

Test calculations

Three kinds of test calculation to verify the FXJH7 libraries were performed using MCNPX.

WNR experiment [9]

The secondary neutron angular-energy spectra from thick iron target bombarded by 256 MeV protons were analysed. Figure 1 summarises the calculation results using LA150, JENDL/HE-2004 and JENDL/HE-2007. Even JENDL/HE-2007 gives slightly higher values at the energy range below 20 MeV, the result gives good agreement as a whole with the experimental data.

TIARA experiment [10]

The energy spectrum of leaked neutron from 2 m thick concrete shield bombarded by 68 MeV p-7Li neutrons were compared with calculation values using LA150, JENDL/HE-2004 and JENDL/HE-2007 as shown in Figure 2. The results using JENDL/HE-2007 give the similar value with other libraries. Then, it is recognised that there are no significant problems for the construction procedure of FXJH7 library by MCNPX calculation. However, further improvements for JENDL/HE-2007 file are indispensable because there are typical discrepancies compared with experimental data.

Figure 1: Comparison of neutron yield from iron target bombarded by 256 MeV protons

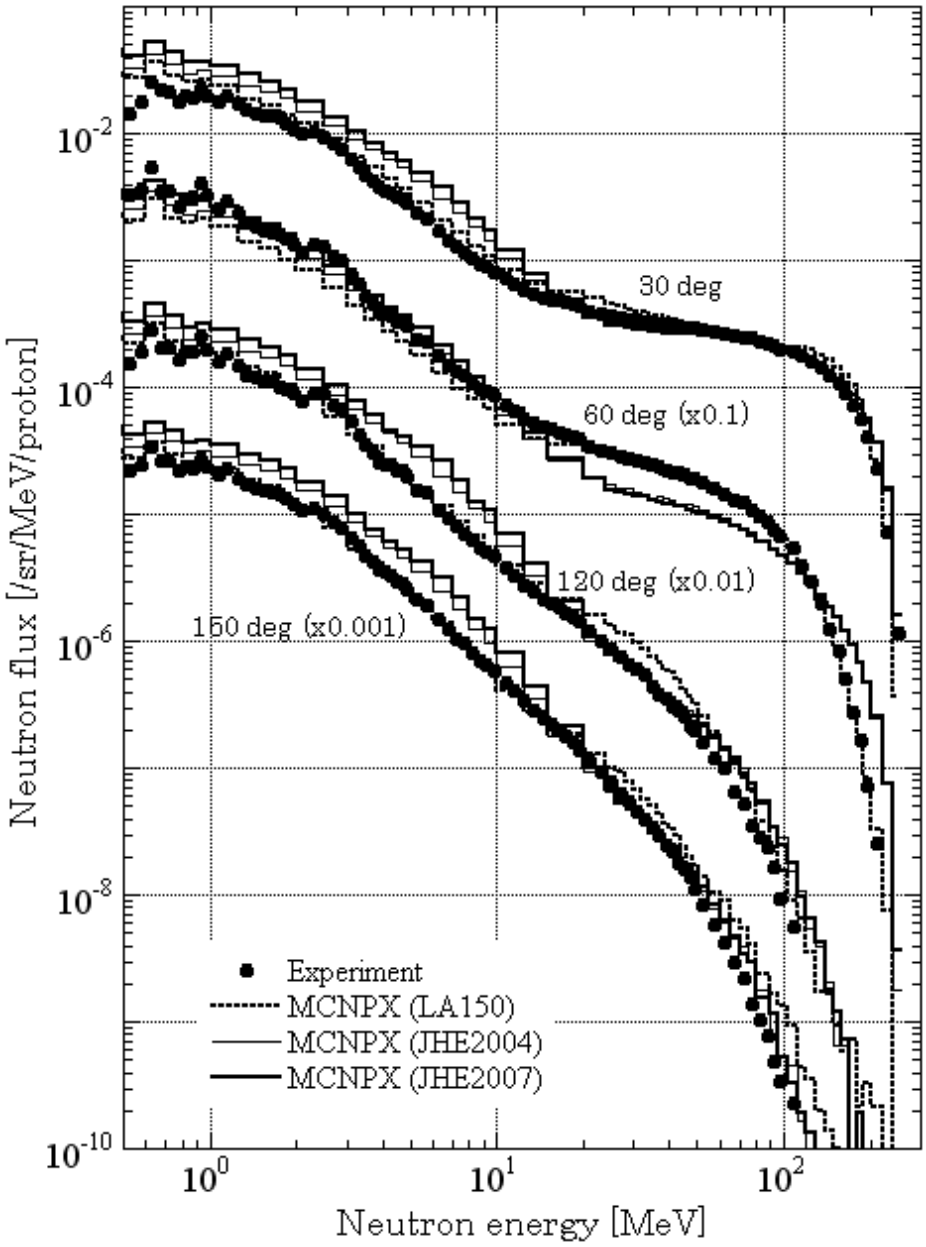

Figure 2: Comparison of neutron spectra on the beam axis behind 2 m-thick concrete slab bombarded by 68 MeV p-^{7}Li neutron

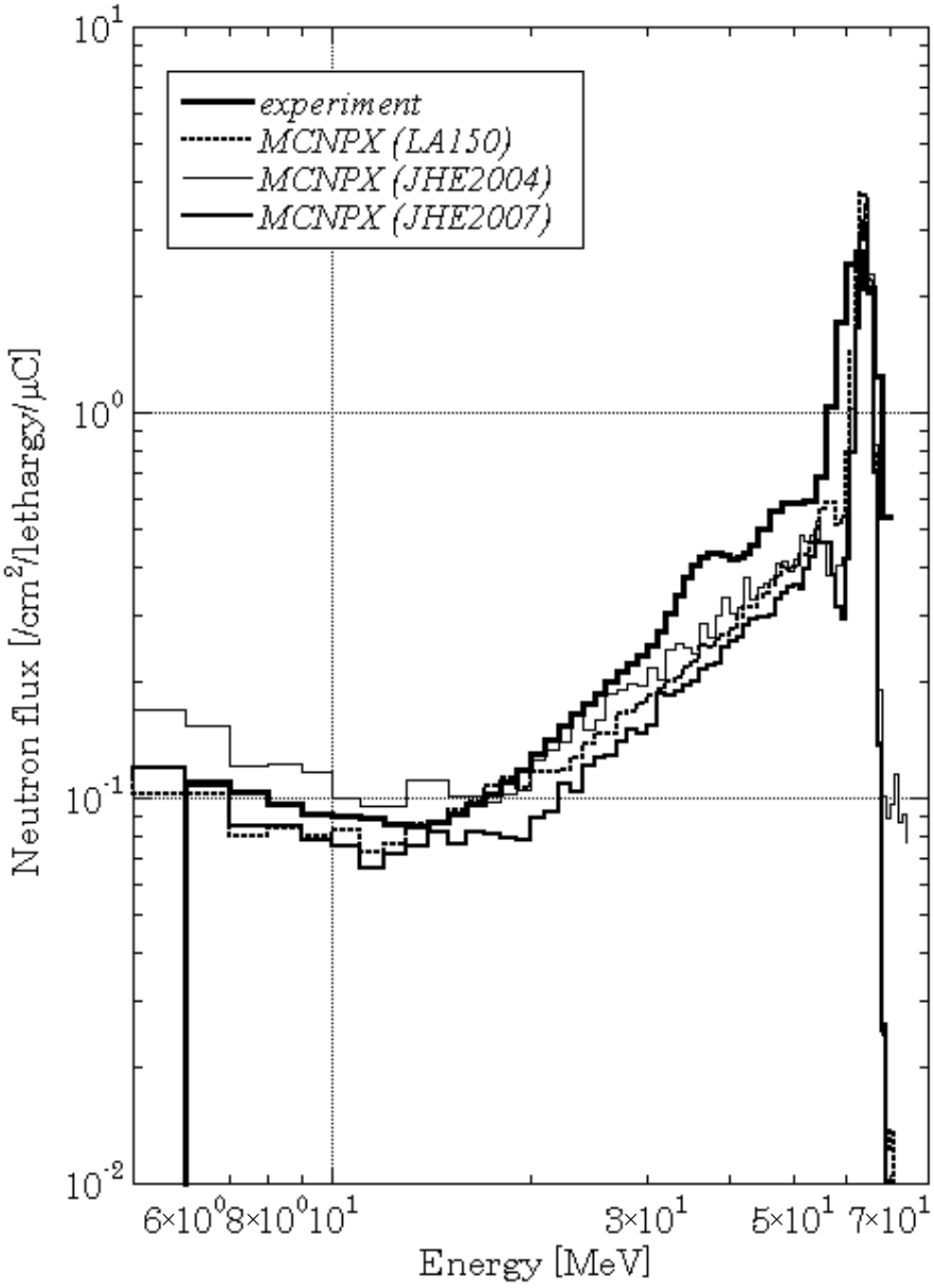

Criticality experiments by small core [11]

Eight kinds of experiments for different target fissile nuclides (JEZEBEL-23 and FLATTOP-23 for ^{233}U core, GODIVA and FLATTOP-25 for ^{235}U core, JEZEBEL, JEZEBEL-Pu, FLATTOP-Pu and THOR-Pu for Pu core) were examined. The analysed results by JENDL/HE-2007 agree well with the calculation results by JENDL-3.3 as shown in Figure 3. In these cases, reflector materials were commonly taken from FSXLIB-J3R2 [12] which is based on JENDL-3.2 [13] because of the existence of materials with natural abundance. This analysis is not essential for the data of additional high energy region but is useful to confirm the validity of NJOY modifications.

Figure 3: Comparison of analysis result for various small core experiments

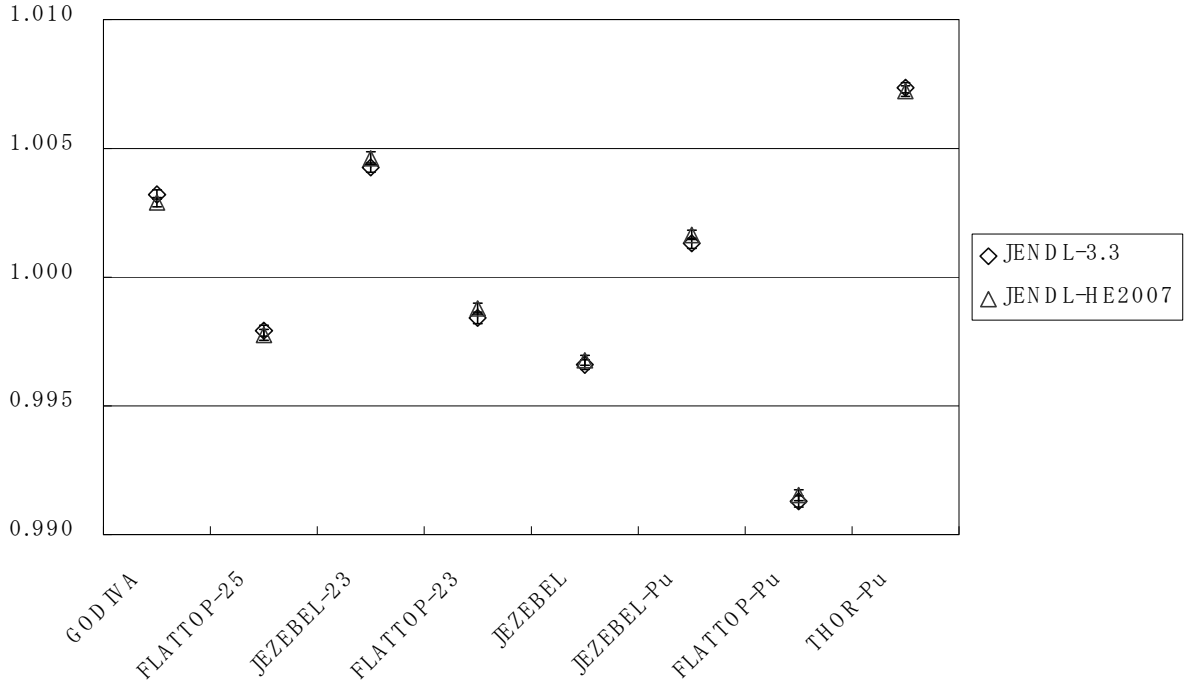

Summary

Continuous cross-section library FSXJH7 was constructed from JENDL/HE-2007. The libraries are prepared for the analysis using the MCNP and MCNPX codes for not only the accelerator related facilities like accelerator-driven system but also the spallation neutron source and the research complex like J-PARC. To perform the analysis in high temperature condition like subcritical core of accelerator-driven system, high energy cross-section libraries for 300°C and 500°C were also constructed together with the data for room temperature (20°C). Validation of the constructed libraries was performed using several kinds of experimental data by shielding analyses and eigenvalue analyses. From the results of the analyses, it is found that the adequate cross-section libraries were produced using modified NJOY.

Acknowledgement

The authors would like to express their thanks to all members of the High Energy Nuclear Data Evaluation Working Group for evaluation and benchmarking of JENDL/HE-2007. This work was done with understanding and co-operation of Dr. Toru Ogawa, the Director General of Nuclear Science and Engineering Directorate and spacious supports by Dr. Hiroyuki Oigawa, the Group Leader of Nuclear Transmutation Technology Group.

References

[1] Chadwick, M.B., *et al.*, "Cross-section Evaluations to 150 MeV for Accelerator-driven Systems and Implementation in MCNPX", *Nucl. Sci. Eng.*, 131, p. 293 (1999).

[2] Hendricks, J.S., *et al.*, *MCNPX Extensions, Version 2.5.0*, LA-UR-05-2675 (2005).

[3] Fukahori, T., *et al.*, "JENDL High Energy File", *J. Nucl. Sci. Technol.*, Suppliment 2, p. 25 (2002).

[4] Fukahori, T., forthcoming (JENDL/HE-2007).

[5] MacFarlane, R.E., D.W. Muir, *The NJOY Nuclear Data Processing System, Version 91*, LA-12740-M, Los Alamos National Laboratory (1994).

[6] Shibata, K., *et al.*, "JENDL-3.3", *J. Nucl. Sci. Technol.*, 39, p. 1125 (2002).

[7] Young, P.G., *et al*, *Comprehensive Nuclear Model Calculations: Introduction to the Theory and Use of the GNASH Code*, LA-12343-MS, Los Alamos National Laboratory (1992).

[8] X-5 Monte Carlo Team, *MCNP – A General Monte Carlo N-particle Transport Code, Version* 5, LA-CP-03-0284 (2003).

[9] Meier, M.M., *et al.*, "Differential Neutron Production Cross-sections for 256-MeV Protons", *Nuclear Science and Engineering*, Vol. 110, p. 289 (1992).

[10] Nakashima, H., *et al.*, "Transmission Through Shield of Quasi-monoenergetic Neutrons Generated by 43- and 68-MeV Protons – II Iron Shielding Experiment and Analysis for Investigating Calculational Method and Cross-section Data", *Nucl. Sci. and Eng.*, 124, p. 243 (1996).

[11] *Cross-section Evaluation Working Group Benchmark Specifications*, BNL-19302 (ENDF-202), Brookhaven National Laboratory (1974).

[12] Kosako, K., *et al.*, *FSXLIB-J3R2: A Continuous Energy Cross-section Library for MCNP Based on JENDL-3.2*, JEARI-Data/Code 94-020 (1994).

[13] Nakagawa, T., *et al.*, "JENDL-3 Revision 2", *Proc. of the 1993 Symposium on Nucl. Data*, JAERI-M 94-019, p. 68 (1994).

Importance of reactor physics experiment using MA-bearing fuel

Takanori Sugawara, Toshinobu Sasa, Hiroyuki Oigawa
Japan Atomic Energy Agency, Japan

Abstract

Research and development (R&D) for minor actinide (MA) transmutation technologies by using fast reactor (FR) and accelerator-driven system (ADS) have been performed at Japan Atomic Energy Agency (JAEA). Improvement on the neutronics design accuracy of the MA-loaded core is one of the most important issues in the MA transmutation technologies. Uncertainties of the current MA nuclear data are supposed to be larger than those of other major nuclides. Therefore, analysed neutronics properties of MA-loaded FR and ADS have much larger design margins in comparison with those of conventional FR. To improve the reliability, safety and economical efficiency of these systems, it is required to increase the accuracy of the nuclear data of MA by the experimental data taken under adequate experimental conditions.

JAEA plans a construction of the Transmutation Physics Experimental Facility (TEF-P) in the second phase of the Japan Proton Accelerator Research Complex (J-PARC) project. TEF-P is a plate-type fuelled critical assembly which is able to accept a proton beam (600 MeV, 10 W) delivered from a linac of J-PARC. Various experiments are available in a critical condition or a subcritical state driven by spallation neutrons. Furthermore, the experiments using pin-type MA fuel, which will be handled with remote devices, are planned to simulate the MA-loaded systems.

In this study, error analyses were conducted to estimate the benefit of the MA-loaded experiments at TEF-P on the error reduction in neutronics design of transmutation systems. In this estimation, the cross-section adjustment procedure with the covariance data prepared in JENDL-3.3 was employed. As a typical result, the errors caused by the nuclear data (the confidence level is 1σ) for the coolant void reactivity were improved from 2.6% to 1.5% for the MA-loaded FR and from 7.4% to 3.5% for the ADS. Through this estimation, the effect of the MA-loaded experiments at TEF-P was verified quantitatively.

Introduction

Research and development (R&D) for minor actinide (MA) transmutation technologies by using fast reactor (FR) and accelerator-driven system (ADS) have been performed at Japan Atomic Energy Agency (JAEA). Improvement of the neutronics design accuracy of the MA-loaded system is one of the most important issues in the MA transmutation technology. Uncertainties of the current MA nuclear data are supposed to be larger than those of other major nuclides. Therefore, analysed neutronics properties of MA-loaded FR and ADS have much larger design margins in comparison with those of conventional FR. To improve the reliability, safety and economical efficiency of these systems, it is required to increase the accuracy of the MA nuclear data by the experimental data taken by adequate experimental conditions.

JAEA plans a construction of Transmutation Physics Experimental Facility (TEF-P) in the second phase of the Japan Proton Accelerator Research Complex (J-PARC) project [1]. TEF-P is a plate-type fuelled critical assembly which is able to introduce a proton beam (600 MeV, 10 W) delivered from the linac of J-PARC. Various experiments are available in a critical condition or a subcritical state driven by spallation neutrons. Furthermore, the experiments using pin-type MA fuel, which will be handled with remote devices, are planned to simulate the MA-loaded systems.

In this study, error analyses were performed to estimate the impact of the MA-loaded experiments at TEF-P on the error reduction in neutronics design of transmutation systems. In this estimation, the cross-section adjustment procedure was employed. By using this procedure, the improvement effect of neutronics design accuracy was demonstrated quantitatively.

Procedure to estimate error caused by nuclear data

The error analyses were performed by the cross-section adjustment procedure [2]. This procedure adjusts the nuclear data to reduce the errors caused by the nuclear data and makes it possible to estimate the errors quantitatively. Figure 1 shows a simplified schematic of this procedure. Existing nuclear data (cross-section T and covariance data M) such as JENDL-3.3 are adjusted by the Bayesian theorem by using sensitivity G, analytical modelling error V_m and experimental error V_e for 233 integral data [3]. The adjusted nuclear data T′ and M′ are calculated as an output.

Figure 1: Procedure to estimate the error caused by the nuclear data

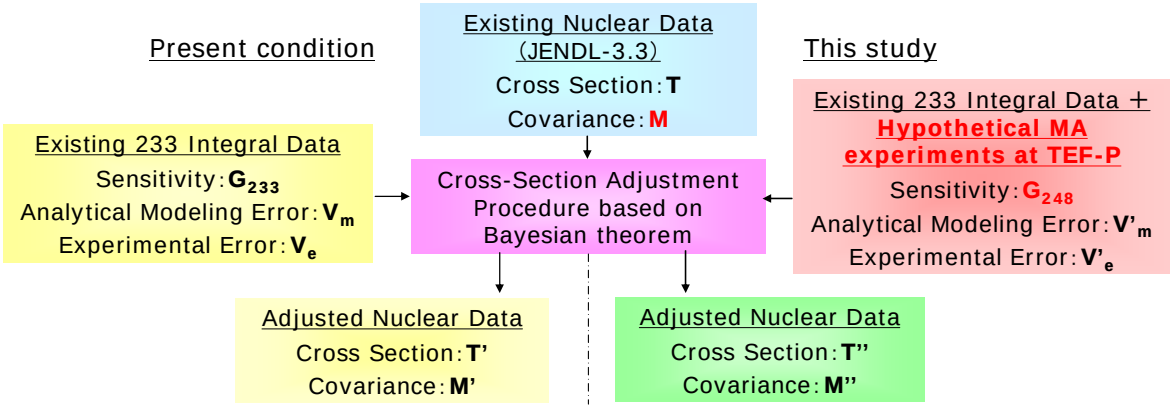

In this theory, the error caused by the nuclear data for a system is defined as $G_{sys}MG_{sys}^t$ (superscript "t" means a transpose) where sensitivity coefficient of the system is defined by G_{sys}. So, it is possible to compare the errors before the adjustment ($G_{sys}MG_{sys}^t$) and those after the adjustment by the 233 integral data ($G_{sys}M'G_{sys}^t$). This procedure also enables us to assess the effect of hypothetical experiments. In this study, hypothetical experimental data using MA at TEF-P were added to the 233 integral data and the error caused by the new adjusted data ($G_{sys}M''G_{sys}^t$) was estimated.

Calculation condition

Object to estimation

The errors included in neutronic designs of the MA-loaded FR and the ADS were estimated. The 3 600 MWt sodium cooled FR core studied in the feasibility study [4] was employed as a typical FR. MOX fuel with 5 wt.% MA was applied to the inner and outer core region of the FR. The composition of MAs was ^{237}Np/^{241}Am/^{243}Am/^{244}Cm = 11.1/44.4/22.2/22.2 wt.% which was the value at the equilibrium cycle of the fast reactor [4]. Figure 2(a) shows the RZ calculation model of the FR core.

Figure 2: RZ calculation model for MA-loaded FR and ADS

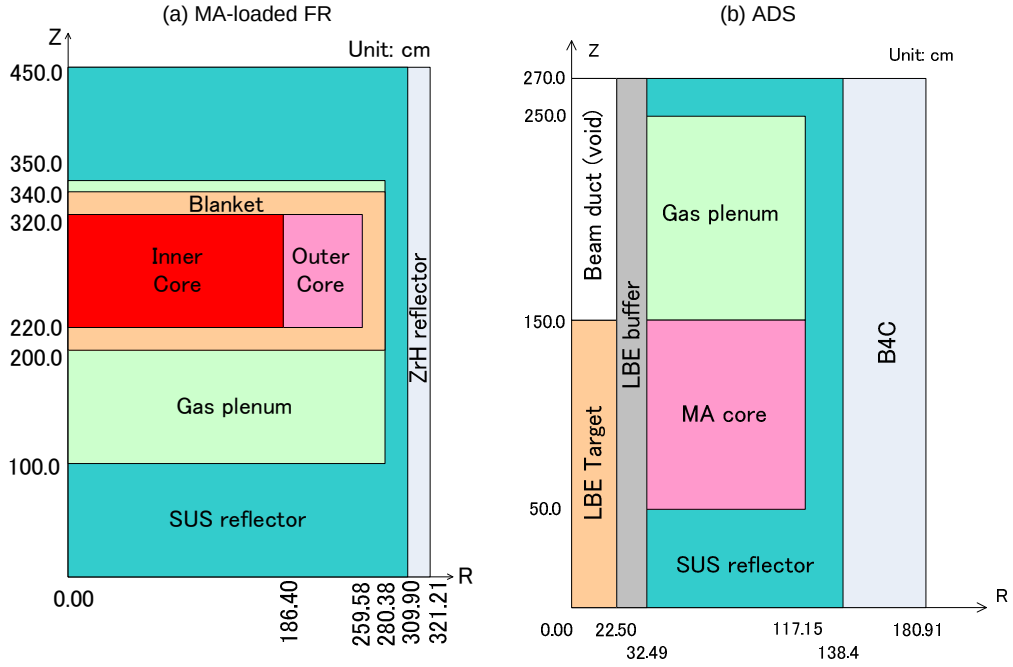

The 800 MWt lead-bismuth eutectic (LBE) cooled ADS designed by JAEA [5] was employed as a typical ADS core. The RZ calculation model for the ADS core is illustrated in Figure 2(b). The composition of MA for the ADS was ^{237}Np/^{241}Am/^{243}Am/^{244}Cm/others = 49.7/32.1/13.4/4.0/0.8 wt.%. Figure 3 compares the weight composition of fuels for the MA-loaded FR and the ADS. The ratio of uranium isotopes is largest in the MOX fuel naturally. For the ADS fuel, the ratios of the inert matrix (ZrN) and MA isotopes are significant.

The sensitivities G_{sys} for the criticality, the coolant void reactivity (coolant volume fraction at the driver region was changed to 0%) and the Doppler reactivity (ΔT = 500 K at the driver region) were calculated for both cores by SAGEP code [6] with 18 energy group structure. Burn-up reactivity was also calculated by PSAGEP code [7] which is the sensitivity analysis code with consideration for the changes of the number density and the power during the operation.

Hypothetical MA experiment

To simulate hypothetical MA experiments, the FCA XVII-1 core [8] which was a mock-up of a MOX fuelled fast reactor was referred. Figure 4 shows the RZ calculation model of the TEF-P core. The characteristic and difference against the FCA core of the TEF-P are that it is available to treat the pin-type MA fuel. The MA fuel pin was loaded in the TEST region (shown in Figure 4). For the FR analysis, U/Pu/MA (= 77.4/17.6/5.0 wt.%) oxide fuel pin surrounded by Na was set to the TEST region. Pu/MA (31/69 wt.%) nitride fuel surrounded by Pb-Bi was set to the TEST region for the ADS analysis.

Figure 3: Weight composition of fuels

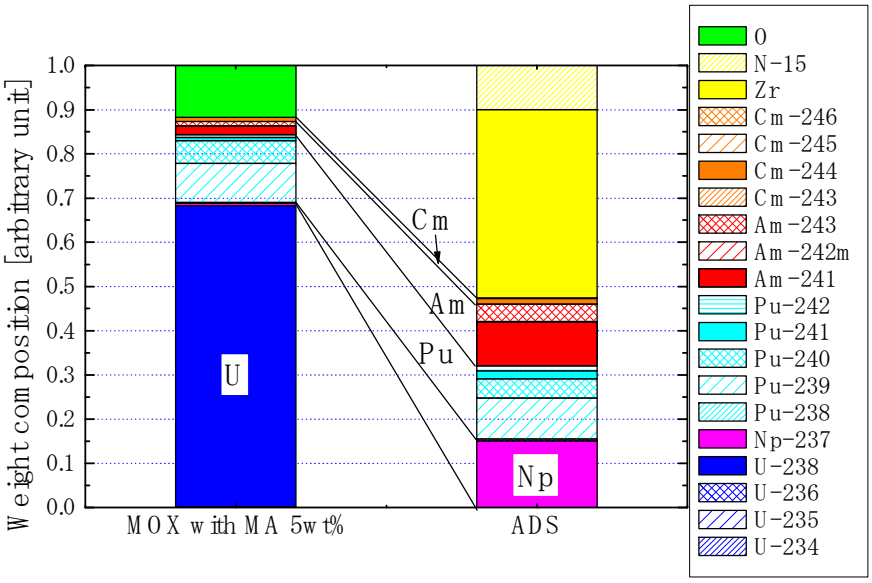

Figure 4: RZ calculation model of TEF-P core (half assembly) based on FCA XVII-1 core [8]

T2: Pu + depleted uranium + Na, DMX: Pu + enriched uranium + Na, SB: UO_2 + Na,
DUB: Depleted uranium block, NUB: Natural uranium block, MTX: Empty matrix

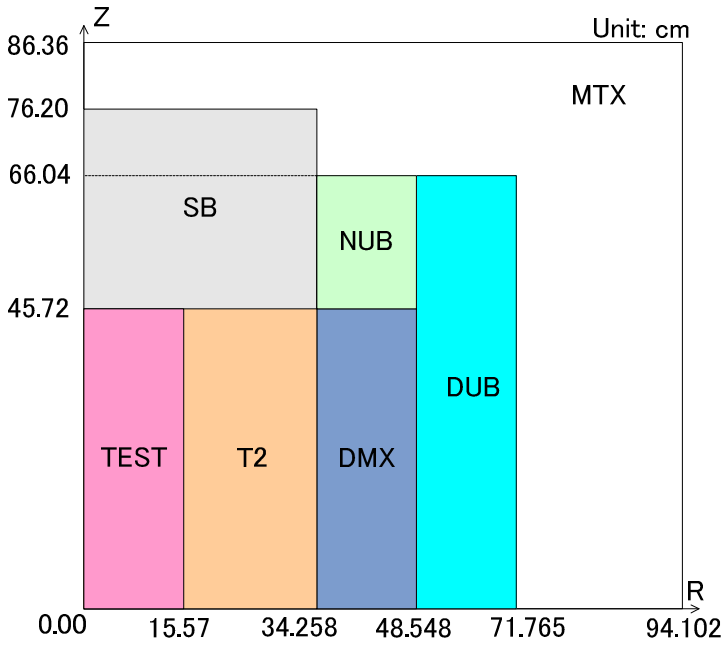

In these calculations, the sensitivities for the hypothetical MA experiments were calculated by the SAGEP code. Fifteen cases were calculated; the criticality (one case), the coolant void reactivity (three cases), the Doppler reactivity (three cases) and reaction rate ratio (eight cases). For the measurement of the reaction rate ratio, it was supposed that the dominator was ^{239}Pu fission reaction and the numerators were fission and capture reactions for four MA nuclides (^{237}Np, ^{241}Am, ^{243}Am and ^{244}Cm). The analytical modelling error V'_m and the experimental errors V'_e were determined based on the FCA XVII-1 experiments (Table 1).

Table 1: Analytical modelling error and experimental error for the TEF-P hypothetical experiments [8]

Case	Analytical modelling error V′m [%]	Experimental error V′e [%]
Criticality	0.04	0.2
Void reactivity (Case 1)	1.0	5.0
Void reactivity (Case 2)	2.0	5.0
Void reactivity (case 3)	3.0	10.0
Doppler reactivity (573 K)	3.0	3.5
Doppler reactivity (823 K)	3.0	4.0
Doppler reactivity (1 073 K)	3.0	4.5
Reaction rate (8 cases)	2.0	5.0

Nuclides and reactions for adjustment

In this study, covariance data which were prepared in the JENDL-3.3 library [9] were used for the adjustment. However, the covariance data for many nuclides and reactions such as capture and elastic scattering reactions for Pb isotopes and ^{209}Bi are not prepared in JENDL-3.3. In the present study, provisional covariance data of these nuclides and reactions [10] were employed. Tables 2 and 3 show the current status of the covariance data required for the MA-loaded FR and ADS analyses. So, errors of all nuclides and reactions (except most of χ and μ-bar data) required for these analyses were considered in this investigation.

Table 2: Nuclides and reactions for adjustment (MA-loaded FR)

Nuclide	Capture	Fission	ν	Elastic	Inelastic	χ	μ-bar
^{235}U	J33	J33	J33	J33	J33	J33	J33
^{238}U	J33	J33	J33	J33	J33	J33	J33
^{238}Pu	J33	J33	p	p	p		
^{239}Pu	J33	J33	J33	J33	J33	J33	J33
^{240}Pu	J33	J33	J33	J33	J33	J33	J33
^{241}Pu	J33	J33	J33	J33	J33		J33
^{242}Pu	J33	J33	p	p	p		
^{237}Np	J33	J33	J33	p	p		
^{241}Am	J33	J33	J33	p	p		
^{242m}Am	J33	J33	p	p	p		
^{243}Am	J33	J33	J33	p	p		
^{242}Cm	p	p	p	p	p		
^{243}Cm	p	p	p	p	p		
^{244}Cm	J33	J33	p	p	p		
^{245}Cm	p	p	p	p	p		
^{246}Cm	p	p	p	p	p		
O	J33	–	–	J33	J33	–	J33
Fe	J33	–	–	J33	J33	–	J33
Cr	J33	–	–	J33	J33	–	J33
Ni	J33	–	–	J33	J33	–	J33
Na	J33	–	–	J33	J33	–	J33

J33: Covariance data prepared in JENDL-3.3.

p: Provisional covariance data [10].

Table 3: Nuclides and reactions for adjustment (ADS)

Nuclide	Capture	Fission	ν	Elastic	Inelastic	χ	μ-bar
^{238}Pu	J33	J33	p	p	p		
^{239}Pu	J33	J33	J33	J33	J33	J33	J33
^{240}Pu	J33	J33	J33	J33	J33	J33	J33
^{241}Pu	J33	J33	J33	J33	J33		J33
^{242}Pu	J33	J33	p	p	p		
^{237}Np	J33	J33	J33	p	p		
^{241}Am	J33	J33	J33	p	p		
^{242m}Am	J33	J33	p	p	p		
^{243}Am	J33	J33	J33	p	p		
^{242}Cm	p	p	p	p	p		
^{243}Cm	p	p	p	p	p		
^{244}Cm	J33	J33	p	p	p		
^{245}Cm	p	p	p	p	p		
^{246}Cm	p	p	p	p	p		
^{15}N	p	–	–	J33	p	–	
Fe	J33	–	–	J33	J33	–	J33
Cr	J33	–	–	J33	J33	–	J33
Ni	J33	–	–	J33	J33	–	J33
^{90}Zr	J33	–	–	p	J33	–	
^{91}Zr	p	–	–	p	p	–	
^{92}Zr	p	–	–	p	p	–	
^{94}Zr	p	–	–	p	p	–	
^{96}Zr	p	–	–	p	p	–	
^{204}Pb	p	–	–	p	p	–	
^{206}Pb	p	–	–	p	J33	–	
^{207}Pb	p	–	–	p	J33	–	
^{208}Pb	p	–	–	p	J33	–	
^{209}Bi	p	–	–	p	J33	–	

J33: Covariance data prepared in JENDL-3.3.

p: Provisional covariance data [10].

Calculation result

MA-loaded FR

Table 4 shows the errors caused by nuclear data for the MA-loaded FR. The error caused by JENDL-3.3 for the criticality was 1.13%. This value was reduced to 0.49% by the adjustment with the existing 233 integral data. Figures 5 and 6 show the breakdown of the errors for the criticality and the burn-up reactivity, respectively. From these figures, it was observed that the errors caused by the nuclear data of ^{238}U and plutonium isotopes were mainly improved by the existing 233 integral data.

Table 4: Error caused by nuclear data (FR)

Case	Value	Error caused by nuclear data (1σ) [%]		
		J33 [b]	^{233}C [c]	^{248}C [d]
Criticality	1.09	1.13	0.49	**0.35 (0.71)** [e]
Coolant void reactivity	3.02×10^{-2} [a]	2.61	1.84	**1.52 (0.83)** [e]
Doppler reactivity	-2.76×10^{-3} [a]	3.89	2.40	**1.79 (0.75)** [e]
Burn-up reactivity	2.16×10^{-3} [a]	166	125	**84.9 (0.65)** [e]

a: Unit [Δk/k], b: JENDL-3.3, c: Nuclear data adjusted by 233 integral data [3], d: Nuclear data adjusted by ^{233}C + 15 hypothetical TEF-P experiments data, e: Relative value against the result of ^{233}C.

Figure 5: Breakdown of the error caused by the nuclear data for the criticality of MA-loaded FR

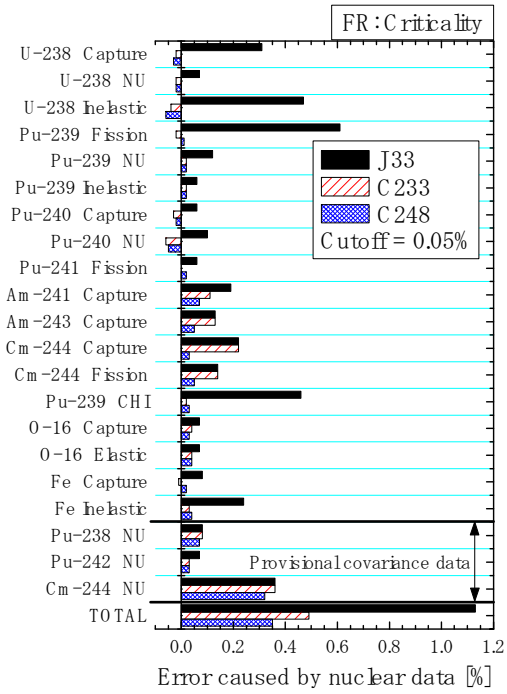

Figure 6: Breakdown of the error caused by the nuclear data for the burn-up reactivity of MA-loaded FR

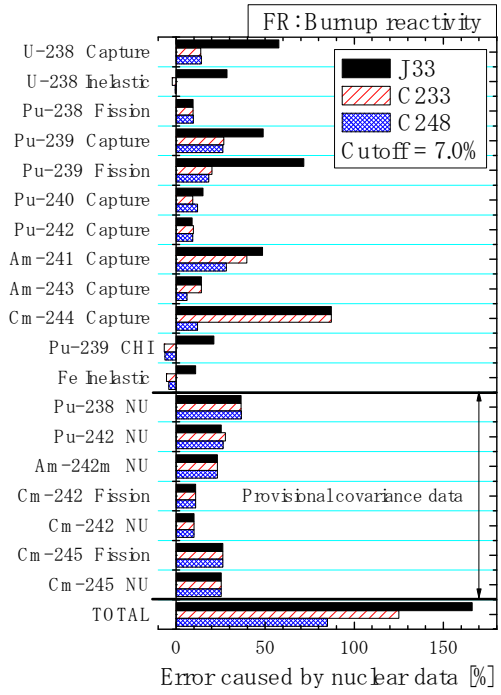

The effect of the MA-loaded critical experiments is also shown in Table 4 and Figures 5 and 6. The error for the criticality was decreased from 0.49% to 0.35% by the adjustment with the 248 integral data which included 15 hypothetical TEF-P experiments data (^{248}C case). Although errors caused by

MA nuclear data such as ^{243}Am and ^{244}Cm were not changed in the ^{233}C case in the breakdown figures, those values were reduced by adding the 15 TEF-P experiments. It was quantitatively confirmed that the MA-loaded critical experiments were useful to reduce the error caused by the MA nuclear data. Meanwhile, the error caused by ^{241}Am capture reaction was improved in the ^{233}C case. This is because the integral data which treated depleted plutonium containing a small amount of ^{241}Am were involved in the existing 233 integral data.

It was also confirmed that errors for other parameters were also improved by the MA-loaded critical experiments. The error caused by the nuclear data was reduced from 1.84% to 1.52% from the ^{233}C case to the ^{248}C case for the coolant void reactivity, from 2.40% to 1.79% for the Doppler reactivity and from 125% to 84.9% for the burn-up reactivity. In this calculation, the maximum reduction of the error was 35% (the burn-up reactivity) from the ^{233}C case by the MA-loaded critical experiments.

ADS

The errors caused by the nuclear data for the ADS are summarised in Table 5. The improvement effect by the MA-loaded critical experiments is also found from this table. The error was reduced from 1.03% to 0.80% for the criticality, from 5.94% to 3.50% for the coolant void reactivity, from 5.22% to 3.33% for the Doppler reactivity and from 46.5% to 45.4% for the burn-up reactivity from the ^{233}C case to the ^{248}C case. The maximum reduction of the error was 41% in the coolant void reactivity by the MA-loaded critical experiments.

Table 5: Error caused by nuclear data (ADS)

Case	Value	Error caused by nuclear data (1σ) [%]		
		J33 [b]	^{233}C [c]	^{248}C [d]
Criticality	0.970	1.30	1.03	**0.80 (0.80)** [e]
Coolant void reactivity	4.87×10^{-2} [a]	7.37	5.94	**3.50 (0.59)** [e]
Doppler reactivity	-1.67×10^{-3} [a]	5.94	5.22	**3.33 (0.63)** [e]
Burn-up reactivity	-2.72×10^{-2} [a]	47.5	46.5	**45.4 (0.96)** [e]

a: Unit [Δk/k], b: JENDL-3.3, c: Nuclear data adjusted by 233 integral data [3], d: Nuclear data adjusted by ^{233}C + 15 hypothetical TEF-P experiments data, e: Relative value against the result of ^{233}C.

Figures 7 and 8 show the breakdown of the errors for the criticality and the burn-up reactivity, respectively. In the ADS case, MA nuclides such as ^{237}Np, ^{241}Am, ^{243}Am and ^{244}Cm mainly contributed to the errors. The errors were reduced by the MA-loaded critical experiments; the contribution of ^{244}Cm capture and fission reactions, particularly, was decreased significantly in the ^{248}C case.

These figures also show that the contribution of the provisional covariance data is indispensable for the error analysis of the ADS. Inelastic reactions for MA in the criticality and ν values for MA and ^{238}Pu were prominent. Especially, the contribution of ^{238}Pu ν value was significant because the amount of ^{238}Pu increased by the capture reactions of ^{237}Np and ^{241}Am in the end of burn-up cycle and the sensitivities of ^{238}Pu (fission, ν and capture) also increased for the burn-up reactivity. These results indicate that it is necessary to develop comprehensive covariance data which obviously includes those provisional covariance data for the error analysis of transmutation systems.

Conclusion

Error analyses were performed to confirm the improvement effect of the MA-loaded critical experiments at TEF-P in J-PARC on the error reduction in neutronics design of transmutation systems. By using the cross-section adjustment procedure, it was quantitatively confirmed that hypothetical MA-loaded critical experiments at TEF-P have a potential to reduce the errors caused by the nuclear data for the MA-loaded FR and the ADS. The error caused by the nuclear data were decreased up to 35% for the MA-loaded FR (the burn-up reactivity) and 41% for the ADS (the coolant void reactivity) from the results of the ^{233}C case by the 15 hypothetical experiments.

MA-loaded critical experiments at TEF-P are important to improve the error caused by the nuclear data for the transmutation systems. It is also important to develop comprehensive covariance data for the error analysis of the transmutation systems.

Figure 7: Breakdown of the error caused by the nuclear data for the criticality of ADS

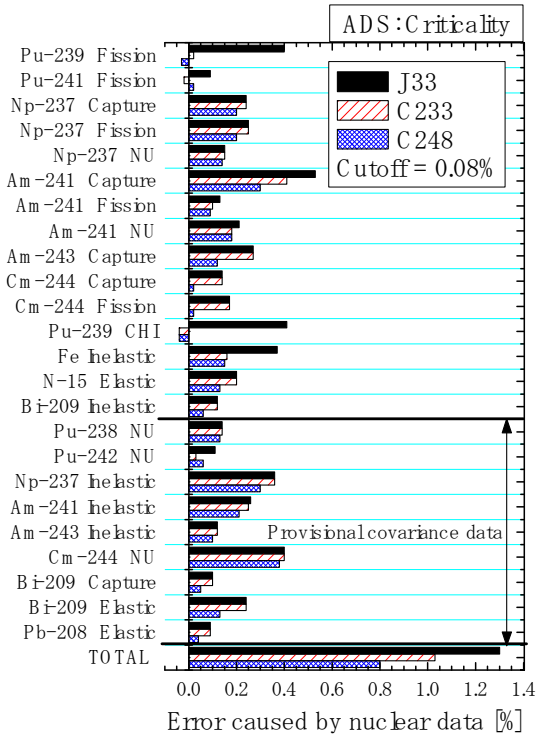

Figure 8: Breakdown of the error caused by the nuclear data for the burn-up reactivity of ADS

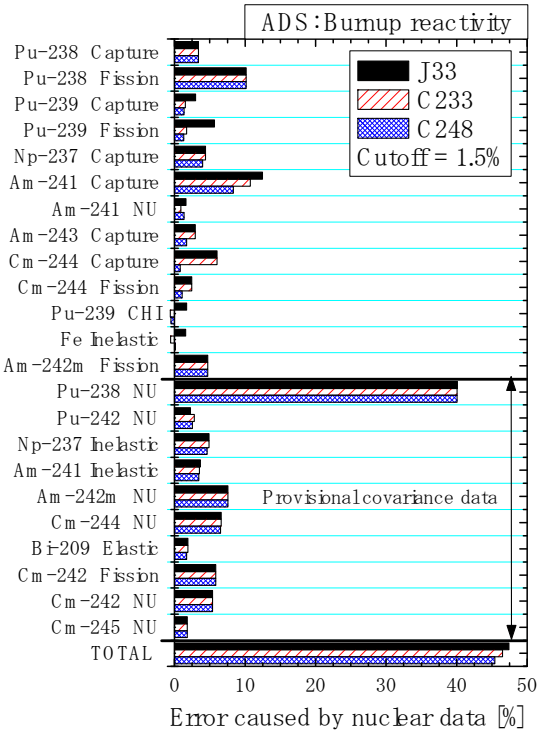

References

[1] Sasa, T., H. Oigawa, "Current Plan of J-PARC Transmutation Experimental Facility", *Proc. of AccApp'07*, Pocatello, Idaho, 29 July-2 August, 949-955 (2007).

[2] Dragt, J.B., *et al.*, "Methods of Adjustment and Error Evaluation of Neutron Capture Cross Sections; Application to Fission Produce Nuclides", *Nucl. Sci. and Eng.*, 62, 117-129 (1977).

[3] Hazama, T., G. Chiba, K. Numata, W. Sato, *Development of the Unified Cross-section Set ADJ2000R for Fast Reactor Analysis*, JNC TN9400 2002-064, Japan Nuclear Cycle Development Institute (JNC) (2002) (in Japanese).

[4] JAEA, *Feasibility Study on Commercialized Fast Reactor Cycle Systems – (1) Fast Reactor Plant Systems*, JAEA-Research 2006-042, Japan Atomic Energy Agency (JAEA) (2006) (in Japanese).

[5] Tsujimoto, K., T. Sasa, K. Nishihara, *et al.*, "Neutronics Design for Lead-bismuth Cooled Accelerator-driven System for Transmutation of Minor Actinide", *J. Nucl. Sci. and Technol.*, 41 [1], 21 (2004).

[6] Hara, A., T. Takeda, Y. Kikuchi, *SAGEP: Two-dimensional Sensitivity Analysis Code Based on Generalized Perturbation Theory*, JAERI-M 84-027, Japan Atomic Energy Research Institute (JAERI) (1984) (in Japanese).

[7] Tatsumi, M., H. Hyoudou, *Systemization of Burnup Sensitivity Analysis Code (II)*, JNC TJ9410 2004-002 (2004) (in Japanese).

[8] Oigawa, H., S. Iijima, T. Sakurai, *et al.*, "A Proposal of Benchmark Calculation on Reactor Physics for Metallic Fueled and MOX Fueled LMFBR Based upon Mock-up Experiment at FCA", *J. Nucl. Sci. and Technol.*, 37 [2], 186 (2000).

[9] Shibata, K., *et al.*, "Japanese Evaluated Nuclear Data Library Version 3 Revision-3: JENDL-3.3", *J. Nucl. Sci. Technol.*, 39 [11], 1125-1136 (2002).

[10] Nakagawa, T., K. Shibata, Private communication (2007).